Handling Qualities of Multirotor RPM-Controlled Electric-Vertical Take-Off and Landing (eVTOL) Aircraft for Urban Air Mobility (UAM)

Carlos Malpica
Aerospace Engineer

Shannah Withrow-Maser
Aerospace Engineer

Aeromechanics Branch
NASA Ames Research Center
Moffett Field, CA, USA

Jeremy Aires
Computer Engineer

Stefan Schuet
Computer Engineer

Intelligent Systems Division
NASA Ames Research Center
Moffett Field, CA, USA

Peter Suh
Aerospace Engineer

Kyle Barnes
Aerospace Engineer

Curt Hanson
Aerospace Engineer

Flight Controls & Dynamics Branch
NASA Armstrong Flight Research Center
Edwards, CA, USA

Allen Ruan
Mechanical Engineer
Science and Technology Corporation
NASA Ames Research Center
Moffett Field, CA, USA

George Altamirano
Research Engineer

John Foster
Research Engineer

Flight Dynamics Branch
NASA Langley Research Center
Hampton, VA, USA

ABSTRACT

A paradigm shift in rotorcraft design is being led by the prospect of propulsive forces being distributed across multiple rotors, such that each rotor can be directly driven by a dedicated electric motor. Crucially, some designers attempt to utilize these direct-drive mechanisms as the sole form of primary flight control. The feasibility of this design choice remains to be proven at the scales required for passenger transport. The paper presents a preliminary handling qualities analysis, for a six-passenger (1,200 lb payload) electric Hexacopter conceptual design, which shows that Level 1 handling qualities for limited agility operations are possible, provided that electric powertrains can deliver transient peak torques twice as high as the rated continuous torque of the conceptual design. Preliminary predictions are then substantiated by the results from a piloted handling qualities evaluation conducted in the NASA-Ames Vertical Motion Simulator (VMS). Three eVTOL configurations (a quadrotor, a hexacopter and a lift+cruise) with flight control laws implementing different levels of stability augmentation (Attitude Command-Attitude Hold and Translational Rate Command response types) were evaluated in four low speed and hover tasks requiring various levels of agility and precision.

NOTATION

Symbols

A	Rotor disk area (ft^2)
c_{d_0}	Airfoil drag coefficient
c_{l_σ}	Airfoil lift curve slope coefficient
$\mathbf{C}(s)$	MIMO command model matrix
f_I	Integral feedback gain fraction
$\mathbf{G}(s)$	Aircraft transfer matrix with rotor speed control
$\mathbf{G}_a(s)$	Bare-airframe aircraft transfer matrix
$\mathbf{H}(s)$	Inner-loop MIMO feedback regulator matrix
$\mathbf{H}_\Omega(s)$	Rotor speed controller feedback matrix
I	Rotational moment of inertia (slug·ft^2)
K	Feedback gain
K_{lat}, K_{lon}	ACAH command model gain parameters (deg)
$\mathbf{L}(s)$	Low-order transfer function approximation of $\mathbf{G}(s)$
p	Body x-axis angular rate (rad/s)
P	Rotor power (ft·lb/s or hp)
q	Body y-axis angular rate (rad/s)
Q	Rotor torque (ft·lb)
Q_{max}	Maximum engine torque at shaft (ft·lb)
Q_{MCP}	Rated continuous torque at shaft (ft·lb)
r	Body z-axis angular rate (rad/s)
r_g	Drivetrain gear ratio
R	Rotor disk radius (ft)
s	Laplace complex frequency domain parameter
$\mathbf{S}(s)$	Feedback sensor transfer functions
t	Time (s)
t_r	Step response rise time (s)
T	Rotor thrust (lb)

T_{DN}	NDARC drivetrain control allocation matrix
$\mathbf{u}_a$	Aircraft inputs (i.e., rotor speed commands)
u	Body x-axis velocity (ft/s)
v	Body y-axis velocity (ft/s)
v_i	Rotor induced velocity (ft/s)
V_{tip}	Rotor hover tip speed, given by ΩR (ft/s)
w	Body z-axis velocity (ft/s)
$\mathbf{y}$	Aircraft response vector
δ	Pilot controller/inceptor input
$\delta_{lat}, \delta_{lon}$	Pilot lateral and longitudinal inputs
δ	Vector of pilot input
ζ_{lat}, ζ_{lon}	ACAH command model damping parameters
θ	Euler pitch attitude (rad or deg)
θ_0	Blade "collective" pitch at 75% radial span (rad)
κ	Rotor induced power correction factor
λ_i	Induced inflow ratio
ρ	Air density (slug/ft^3)
σ	Rotor solidity
σ_w	Vertical turbulence intensity (ft/s)
τ_e	Diagonal matrix of equivalent time delays (s)
τ_M	Motor torque (ft $\cdot$ lb)
τ_p	Phase delay (s)
ϕ	Euler roll attitude (rad or deg)
ψ	Euler yaw attitude (rad or deg)
ω_{BW}	Small-amplitude response bandwidth (rad/s)
$\omega_{lat}, \omega_{lon}$	ACAH command model natural frequency parameters (rad/s)
ω_{onset}	Limit onset frequency (rad/s)
Ω	Rotor speed (rad/s)
Ω_0	Trim rotor speed (rad/s)
Ω_i	Rotor speed for i-th rotor (rad/s)

Key Acronyms

ACAH	Attitude Command-Attitude Hold
eVTOL	electric Vertical Take-Off and Landing
EMC	Electric Motor Controller
HQR	Handling Qualities Rating
HQTE	Handling Qualities Task Element
MCP	Maximum Continuous Power
MTE	Mission Task Element
OLOP	Open-Loop Onset Point
PFC	Primary Flight Control
PMSM	Permanent Magnet Synchronous Motor
RSC	Rotor Speed Controller
TRC	Translational Rate Command
VMS	Vertical Motion Simulator

INTRODUCTION

The emergence of rotorcraft electric propulsion technologies is enabling new, revolutionary, types of Vertical Take-Off and Landing (VTOL, or more specifically, eVTOL) vehicles, intended for Urban Air Mobility (UAM) operations (Refs. 1–3). As a concept of operations, UAM envisions the transport of people or goods at lower altitudes within densely populated urban and suburban areas (Refs. 4, 5). These novel rotorcraft types generally tend to have high(er) numbers of rotors to distribute the propulsive loads, with direct-drive to individually control the speed (RPM) and thrust of the rotors, and, uniquely, some designers attempt to utilize these direct-drive mechanisms as the sole form of primary flight control.

The potential savings in vehicle gross weight, for a given payload, and the reduction in mechanical complexity (and associated maintenance cost savings) that can be achieved by eliminating the swashplate mechanisms has made the use of rotor speed for primary flight control (RPM control) an attractive option amongst eVTOL designers. This vehicle design approach fully integrates the propulsion and flight control systems, with the vehicle engines[1] now also serving as the primary flight control actuators. The implications of this design choice on the attainable control power are not fully understood; yet, ensuring the installed engine torque and power margins can produce the control power to meet the mission-based operational agility and stability requirements can have a profound effect on the vehicle design. Previous analytical studies (Refs. 6–10) have looked at the effect of vehicle scale and found significant limitations for full-scale UAM multirotor configurations using RPM control only to achieve Level 1 handling qualities (HQ) requirements. In Refs. 6–8, power-train limits were shown to significantly degrade flight control system performance. Walter et. al. (Ref. 9) then systematically increased the scale of a quadrotor configuration, up to a gross weight of 1,200 lb (544 kg gross mass), achieving optimal use of the control power for various levels of stability augmentation (response type). These studies suggested that increasingly larger motor weight fractions would be required with increasing vehicle scale for higher stability augmentation control modes. Reference 10 showed that little improvement in handling qualities would be achieved (on the 6-passenger Hexacopter) by varying the trim control allocation to the rotors, without significantly increasing the installed power of the design.

Most studies to date have been limited to predictive handling qualities criteria, based on Aeronautical Design Standard-33 (ADS-33) military standards (Refs. 11, 12), or relied on oversimplified motor models. While ADS-33 does provide a powerful framework to aid in the design of both aircraft and flight control systems, quantitative design criteria may not be directly applicable to UAM. The possibly differing agility and stability requirements of the mission needs to be considered when specifying the predictive handling qualities metrics. A piloted handling qualities simulation experiment of the heave disturbance rejection and control response characteristics of eVTOL quadrotors using RPM control (Ref. 13) showed significant sensitivity of the handling qualities to the variations in the aggressiveness and precision demands relative to the baseline requirements from ADS-33. Relevantly, the FAA has been simultaneously developing an approach to certification that mirrors ADS-33 in many ways (Refs. 14, 15). Key to this framework is the adoption of a Mission Task Element (MTE) flight-testing approach (Handling Qualities Task Element, or

---

[1]In the context of RPM control, engines refer specifically to the electric machines that drive, and are used for controlling the rotational speed of, the rotors.

HQTE, in FAA parlance) to vehicle certification. The proposed framework remains in draft form, however, and specific HQTE requirements have not yet been officially established.

Analysis of power usage from quadrotor configurations using RPM control with unlimited-power engine models in Ref. 13 showed that vehicles drew significant (1.5–3.6 times the rated maximum continuous power, or MCP, of the largest engines) peak power per engine to maneuver (Ref. 16), primarily in tasks that required lateral or longitudinal control. This result emphasizes the potential agility limitations that may arise from using RPM control only. Electric powertrain systems involve significant complexity, however, with motor torque or power output limits that may arise from the exceedance of the capabilities of individual components in the electrical system caused by the rotor dynamic loads during transient maneuvers (Ref. 17).

The objective of this study was to investigate hover and low speed handling qualities of RPM-controlled eVTOL aircraft with increased-stability flight control augmentation (attitude and translational rate response types), under UAM mission-representative maneuvering requirements. This objective was supported by a pilot-in-the-loop handling qualities simulation study in the NASA-Ames Vertical Motion Simulator (VMS) using various UAM multirotor eVTOL configurations. A similar capability to that of Ref. 17, specifically modeling permanent magnet synchronous motor (PMSM) propulsion systems, was developed to realistically assess the effect of control power limitations on the handling qualities of these configurations.

LIMITING OF ROTOR SPEED CONTROL

Nonlinearities in the aircraft dynamics, such as those associated with actuator rate limiting, are known to be a major factor in the development of unfavorable, often severe, aircraft-pilot coupling (APC) events, such as Category II and Category III Pilot Induced Oscillation (PIO) (Ref. 18). This section is not intended as an in-depth discussion of PIO, but rather to discuss the nonlinear (quadratic) aspects of rotor speed control and how these play into the mechanisms of saturation. The section will touch on the applicability of linear prediction techniques, mainly the Open-Loop Onset Point (OLOP) criteria, and how available control power may limit the handling qualities response type criteria.

Typically, when an actuator reaches a saturation or a rate limit, this limits the magnitude or the rate of application, respectively, of the aircraft control forces and moments. This manifests as a reduction in the open-loop frequency-response magnitude or an increase in the phase delay. For multirotor VTOL aircraft that do not use cyclic pitch, the forces and moments required to control heave, roll and pitch are typically produced through the combination of thrust from the various rotors. Yaw control would result from the combination of torques from individual rotor shafts resulting in a non-zero net yaw moment. Fundamentally, the rate limiting mechanism of a multirotor VTOL heave, lateral and longitudinal control can be viewed through the lens of the thrust limits. In particular,

the rate limiting mechanism can be viewed as a limit of the rate of application of thrust, or $\dot{T}$.

Based on simple blade element momentum theory (BEMT), rotor thrust within the linear range of the airfoils is given by

$$T = \frac{1}{2}\sigma c_{l_\alpha}\rho A V_{tip}^2 \left(\frac{\theta_0}{3} - \frac{\lambda_i}{2} \right), \qquad (1)$$

For *fixed speed* rotors, one can conclude from Eq. 1 that $T \propto \theta_0$, and that, to first-order approximation (i.e., assuming quasi-steady inflow), $\dot{T} \propto \dot{\theta}_0$. It can be seen that an actuator reaching a rate limit would limit the rate of change of thrust, and therefore also the rate of change of the control moments the rotor can exert on the vehicle. This effect is analogous to what would be observed during the rate limiting of the control surface actuator on an airplane.

For *fixed pitch* rotors, $T \propto \Omega^2$, such that $\dot{T} \propto \Omega\dot{\Omega}$. The problem of determining the actuator rate limits is fundamentally nonlinear. Rotor acceleration $\dot{\Omega}$ limits are necessary but not sufficient to characterize the thrust rate limit. Critically, the rate of application of thrust is a function of the operating state of the rotor. Low operating speed of the rotors, for example, could potentially be conducive to lower rates of thrust application, for a given torque margin.

Torque Limiting

Contrary to fixed speed rotors, where increasing the collective can cause the blades to stall, increasing the rotor speed in a rotor with fixed pitch causes a reduction in the local aerodynamic angles on the blades. This moves the rotor further away from stall. Control limits need to be explained in terms of the drivetrain power and torque limits. Aerodynamically, as long as installed power can be applied at the shaft to match the required power, the rotors can in general be sped up to any speed (barring structural or aeroelastic limits).

Figure 1 illustrates the fundamental characteristics of a rotor response to maximum shaft torque Q_{max}. A characteristic recognized by Walter et. al. (Ref. 9), the maximum rotor acceleration at the onset of the saturation is essentially given by

$$\dot{\Omega}_{max} = \frac{Q_{max} - Q(\Omega_0)}{I_R}. \qquad (2)$$

where Ω_0 is the initial rotor speed and I_R the moment of inertia. As rotor speed increases, though, so does the load on the motor. Maximum rotor speed Ω_{max} is achieved when the rotor torque load equals the drivetrain torque. Simultaneously, rotor acceleration approaches zero, such that

$$\lim_{t \gg t_r} \dot{T} = 0.$$

Rotor aerodynamic torque was derived from the power by

$$Q = \frac{P}{\Omega}$$

where

$$P = \kappa T v_i + \frac{1}{8}\sigma c_{d_0}\rho A V_{tip}^3$$

3
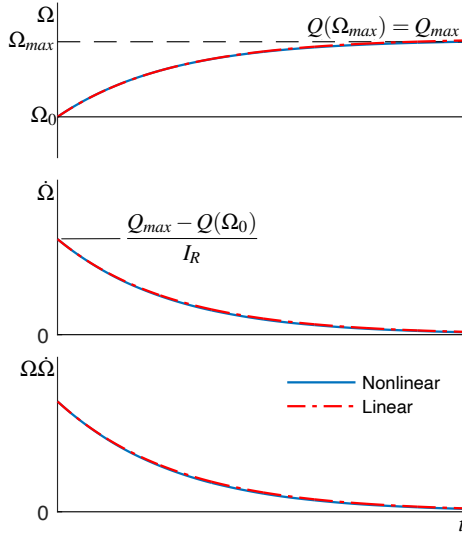
Figure 1. Notional rotor response to maximum engine torque step change.

from BEMT in hover. Unsteady induced velocity effects were taken into account using the following approximation by Carpenter and Friedovitch (Ref. 19):

$$0.637\rho\frac{4}{3}A\dot{v}_i = -2\rho Av_i^2 + T.$$

Calculations behind Figure 1 are for an arbitrary, but UAM-representative, rotor geometry. At this junction the specifics are not important. Figure 1 illustrates some key fundamental aspects: 1) reduced control margin for higher trim thrust (reflected in higher Ω_0), 2) dependency of the onset acceleration limit on the initial condition (lower for higher initial thrust), and 3) minimal effect of Ω^2 nonlinearity. Practically overlaid on each other are the rotor linearized and nonlinear responses from BEMT, suggesting the linear approximation could in fact provide an accurate representation of the rotor response dynamics.

Open-Loop Onset Point (OLOP) and Prediction

OLOP criteria was proposed by Duda (Ref. 20) for predicting the likelihood of closed-loop instability of the coupled pilot-vehicle dynamics that may be triggered by nonlinear, rate limited, control elements in the open-loop path in highly augmented fixed wing aircraft. The OLOP criteria has been reexamined more recently for application to rotorcraft by Jones (Ref. 21), and applied to the analysis of RPM-controlled UAM quadrotor configurations by Walter et. al. (Ref. 9). The basis for the criteria is rooted in the Nichols margin criteria, with the prevailing idea being that likelihood of instability correlates with the loss of phase and amplitude margin that is observed after rate limiting onset. This relies on the identification of the onset frequency at which the saturation nonlinearity is activated.

Identification of the onset frequency relies on, and is specific to, the closed-loop controller. It is however instructive to take a look at the potential variation of the onset limit with respect to drivetrain torque limits and rotor operating condition. Results from Figure 1 suggested that a linear approximation of the rotor response would be sufficiently accurate to allow for control system design and analysis. When considering the perturbation dynamics around trim, it follows from Eq. 1 that $\delta\dot{T} \propto \Omega_0\delta\dot{\Omega} + \delta\Omega\dot{\Omega}_0$. For a trimmed initial condition, $\dot{\Omega}_0 = 0$, such that $\delta\dot{T} \propto \Omega_0\delta\dot{\Omega}$. The rate of application of thrust is still dependent on the trim rotor speed, and hence the flight condition.

While the linear approximation can be accurate for analysis at a single flight condition, a thorough assessment of the likelihood of instability caused by saturation or rate limiting of the drivetrain for a given configuration calls for a more general approach or, at least, the identification of a worst case scenario. This may be difficult, given the potential complexity of eVTOL electric powertrains. Consider however some simple example cases based on the Hexacopter from Ref. 10. Sized using the NASA Design and Analysis of Rotorcraft (NDARC) tool (Ref. 22), the design employed six identical electric drivetrains with a rated maximum continuous power of 87 hp (64 kW) each. Given the assumed 8,000 rpm specification speed of the motor model, the engines were rated at 57.1 ft-lb (76.4 Nm) continuous operation torque.

Engines would rarely be subjected to sustained step-like inputs such as in Figure 1 when used as actuators during maneuvering flight. Rather, the flight control system will request large torque pulses in response to the pilot maneuver commands. The magnitude and duration of these pulses would depend on the required aggressiveness of the maneuver. This is so rotors can be accelerated within the relatively short timescales required for primary flight control. A key question for RPM-controlled eVTOL has to be what peak torques can be delivered by the engines during short term or intermittent operation. Figure 2 shows the rotor response to various torque pulses of 1 s duration. Limiting the drivetrain torque output to the rated continuous torque, Q_{MCP} at the rotor shaft, resulted in minimal rotor speed changes for this rotor configuration and trim condition. Such a torque ratio would be unlikely to produce acceptable handling qualities. Allowing the maximum shaft torque, Q_{max}, to achieve twice the rated continuous torque enabled a rotor speed change of about 8 rad/s, and a much more promising handling qualities solution achieving a 38% thrust change relative to the trim thrust (remembering the quadratic relationship of the thrust to the rotor speed).

Effect of vehicle weight (for $Q_{max} = 2Q_{MCP}$) is illustrated in Figure 3. The rotor at the lowest initial thrust condition (empty configuration) possessed the highest overall control authority, allowing a rotor speed change of about 9–10 rad/s or a 50% thrust change. This was about 25% higher than the thrust change achieved by the more heavily loaded rotor (5–6 rad/s rotor speed change).

A trade-off between Ω_0 and $\dot{\Omega}_{max}$ was observed, however, that partially offset the overall thrust rate application capability (as
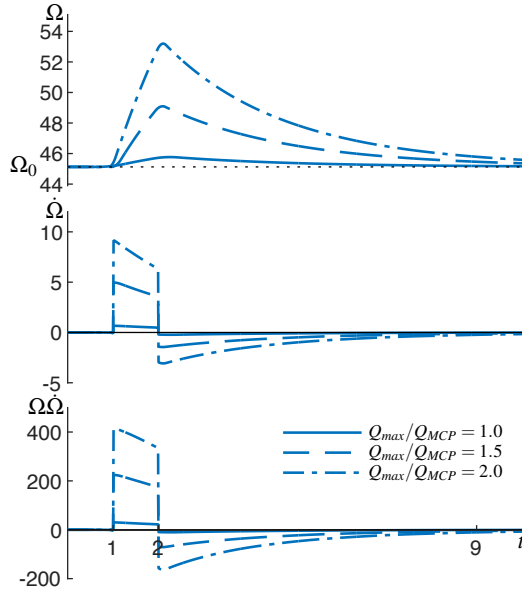
Figure 2. Effect of torque limiting on saturation onset.

Figure 3. Effect of thrust on saturation onset.

determined by the product $\Omega_0 \dot{\Omega}_{max}$). While Ω_0 increased with respect to the initial rotor loading, the maximum acceleration $\Omega_0 \dot{\Omega}_{max}$ for the lightly loaded rotor was about 56% higher (10–11 rad/s^2) than for the heavily loaded rotor (6–7 rad/s^2). Overall, this resulted in maximum thrust rate difference of about 25%.

Integrated Handling Qualities Analysis

A flight control law optimization analysis was conducted using the CONtrol Designer's Unified InTerface (CONDUIT) software (Ref. 23) to investigate the integrated effect of torque limits on the inter-connection between response type handling qualities specifications (bandwidth and agility) and OLOP criteria for the UAM Hexacopter.

Control laws were synthesized based on an explicit model-following control system architecture, shown in Figure 4. Figure 4a illustrates the key elements of the flight control system. The architecture offers a tractable method for independent feedback stabilization and command shaping for the heave, roll, pitch and yaw axis. A command model $\mathbf{C}(s)$ interprets pilot inputs δ, shaping them into a desired vehicle response $\mathbf{y}_{des}$. $\mathbf{L}(s)$ is a low-order equivalent system (LOES) approximation of the open-loop aircraft rate dynamics $\mathbf{G}(s)$, over a desired frequency range of interest (1–10 rad/s, in this instance). This feed-forward component provides lead compensation through the inversion of the LOES model, estimating input $\mathbf{u}_a$ to achieve the desired response. The role of the regulator $\mathbf{H}(s)$ is, firstly, to guarantee stability of the aircraft, and secondly, to ensure accurate tracking of the command by minimizing the error between commanded and measured output (via sensors $\mathbf{S}(s)$).

Hidden underneath the high-level description of Figure 4a are

the rotor speed controller details internal to $\mathbf{G}(s)$. The basic elements—a pre-defined control allocation matrix, T_{DN}; a rotor speed error feedback compensator, $\mathbf{H}_\Omega(s)$; the engine and engine speed controller; and the bare-airframe aircraft aerodynamic model, $\mathbf{G}_a(s)$—are shown in Figure 4b. Here, rotor speed signals were fed back and compared against commanded speeds from the allocation matrix T_{DN} to determine rotor speed error signals. The rotor speed control compensator $\mathbf{H}_\Omega(s)$ specifies torque commands required to regulate rotor speeds with minimal error. The engine torque controller units are high-bandwidth electric components that respond at frequencies much higher than those required for flight control. Neglecting the electrical complexities of motor control, this was assumed to behave as a saturation element for purposes of the CONDUIT optimization problem. In the linear dynamics domain, the motor controller was assumed to deliver commanded torque within limits determined by:

$$Q_{upper} = Q_{max} - Q_0 \tag{3}$$
$$Q_{lower} = -Q_0$$

where Q_0 is the trim shaft torque.

Feedback synthesis Inner-loop and rotor speed feedback matrices are

$$\mathbf{H}(s) = \begin{bmatrix} H_w(s) & 0 & 0 & 0 \\ 0 & H_\phi(s) & 0 & 0 \\ 0 & 0 & H_\theta(s) & 0 \\ 0 & 0 & 0 & H_\psi(s) \end{bmatrix}$$

and

$$\mathbf{H}_\Omega(s) = \begin{bmatrix} H_\Omega(s) & \cdots & 0 \\ \vdots & \ddots & \vdots \\ 0 & \cdots & H_\Omega(s) \end{bmatrix}$$

5

(a)

(b)
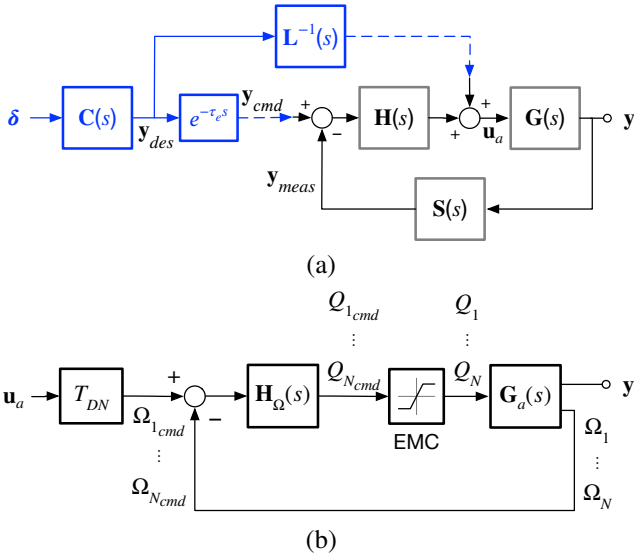
Figure 4. Model-following control system: (a) general architecture, and (b) rotor speed control loops.

respectively, where

$$H_w(s) = K_w \left(1 + \frac{f_{I_w}}{s} \right) \tag{4}$$

$$H_\phi(s) = K_p s + K_\phi \left(1 + \frac{f_{I_\phi}}{s} \right) \tag{5}$$

$$H_\theta(s) = K_q s + K_\theta \left(1 + \frac{f_{I_\theta}}{s} \right) \tag{6}$$

$$H_\psi(s) = K_r s + K_\psi \left(1 + \frac{f_{I_\psi}}{s} \right) \tag{7}$$

$$H_\Omega(s) = K_{P_\Omega} + \frac{K_{I_\Omega}}{s} \tag{8}$$

The problem of synthesizing the optimal feedback gains (from Eqs. 4–8) in CONDUIT was defined by specifying constraints according to Table 1. Absolute (eigenvalue real part) and relative (phase, gain and Nichols margins) stability requirements were established as hard constraints, which must be met for the synthesized control law to be feasible. In addition, rotor speed steady-state tracking error was defined as a hard constraint to guarantee accurate speed scheduling, even under variable or uncertain loading conditions. Soft constraints included the rotor speed and aircraft mid-term transient responses (damping), disturbance rejection criteria (Ref. 12), and minimum crossover frequencies. Minimum crossover frequency constraints, while not standard requirements, enforced basic rules of thumb that ensure minimum steady-state tracking performance. OLOP specifications were configured to predict the onset of rotor acceleration limiting, based on maximum acceleration $\dot{\Omega}_{max}$ from Eq. 2. Application of the OLOP criteria here was extended to disturbance inputs, and normalized by 10 ft/s (heave) and 5 deg (roll and pitch) maximum input magnitudes. Summed objectives included the crossover frequencies (for each axis) and engine usage specifications (for motors 1, 3 and 5). The latter specifically calculate the square root of the integrated spectral density function of the

Table 1. Feedback Optimization Constraints.

Specification	Requirement	Loop[a]
Hard Constraints		
Eigenvalue stability	$\text{Re}(\lambda) < 0$	All
Steady-state error	0.5 dB	RSC
Gain Margin	6.0 dB	All
Phase Margin	45 deg	All
Nichols Margins	Special	PFC
Response damping	0.9	RSC
Soft Constraints		
Eigendamping (0.5–4 rad/s)	0.35	All
Eigendamping (4–20 rad/s)	0.2	All
DRB	1.0 rad/s	Heave
DRB	0.9 rad/s	Roll
DRB	0.5 rad/s	Pitch
DRB	0.7 rad/s	Yaw
DRP	5.0 dB	PFC
OLOP	Special	PFC[b]
Min. crossover frequency	0.5 rad/s	Heave
Min. crossover frequency	2.5 rad/s	Roll
Min. crossover frequency	2.0 rad/s	Pitch
Min. crossover frequency	0.5 rad/s	Yaw
Min. crossover frequency	4.0 rad/s	RSC
Summed Objectives		
Max. crossover frequency	10 rad/s	All
Actuator RMS[c]	1.5	All

[a]PFC = Primary Flight Control, RSC = Rotor Speed Control
[b]Not applied to yaw axis
[c]Motors 1 (front right), 3 (middle right) and 5 (rear right)

engine torque output, normalized by the same maximum disturbance input magnitudes used with the OLOP specifications and torque output magnitudes (Eq. 3). This allowed the optimizer to quantify the engine torque response to heave, roll, pitch and yaw disturbance inputs over the entire frequency range of interest for control. This approach ensured that handling qualities requirements were achieved with minimal control authority (i.e., minimal engine torque required).

Maximum to rated continuous torque ratios of 1 and 1.5 were insufficient to achieve RMS values less than 1.5 for all axes. The actuator RMS metric is not a standard specification, but it does represent basic rules of thumb, and using it as a summed objective is good practice. The presumption here was that an RMS greater than 1.5 will have a high likelihood of exceeding a limit. This approach guaranteed the optimizer had some mechanism to minimize usage of the engines. Without rigorous design margin optimization, the torque ratio was set to 2 for solution shown in Figure 5. One immediate observation is that rejection of heave and yaw disturbances drew significantly higher torques. Comparatively, and subject to the arbitrary maximum disturbance input normalization parameters, roll and pitch disturbance rejection used only about 20% of engine torque. Finally, the resulting crossover frequencies for the primary flight control axes ranged from 1 to 2.6 rad/s (Figure 6).
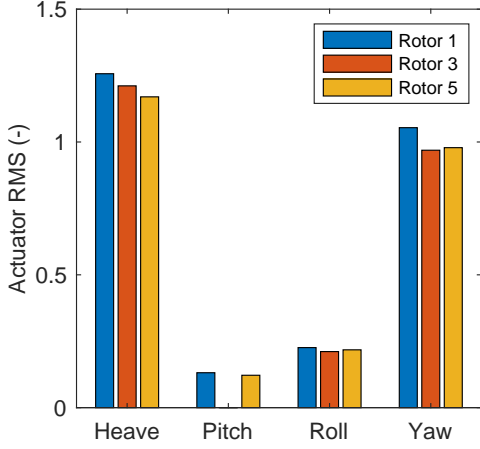
Figure 5. Motor torque usage for disturbance rejection specifications.
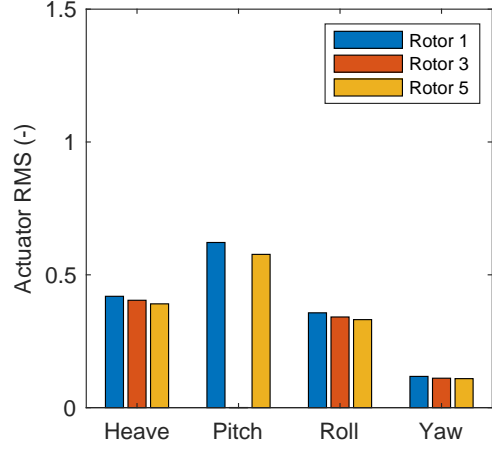
Figure 7. Motor torque usage for limited agility response type specifications.
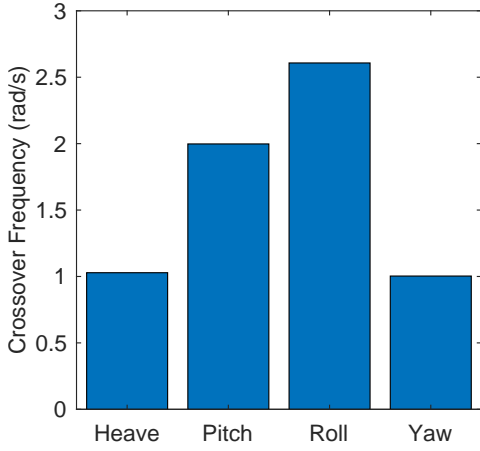
Figure 6. Crossover frequencies.

Feedforward synthesis Synthesis of the feedforward components required the estimation of LOES inverse models $\mathbf{L}(s)$ and delays τ_e be accomplished after the synthesis of the feedback control laws was completed. This deviation from the classical approach was made necessary because the specific mechanization of the control laws rendered the rotor speed loops integral to the aircraft dynamics $\mathbf{G}(s)$, and these were unknown a priori. Moreover, the feedback optimization resulted in rotor speed control loop crossover frequencies within the 1–10 rad/s range (about 4.8 rad/s). This is a generally undesirable characteristic, but a consequence of using rotor speed for primary flight control and choosing to minimize demand on the engine torque output.

Command shaping for roll and pitch Attitude Command-Attitude Hold (ACAH) response types was achieved through the definition of second-order filters:

$$\frac{\phi_{des}}{\delta_{lat}} = C_\phi(s) = \frac{\omega_{lat}^2 K_{lat}}{s^2 + 2\zeta_{lat}\omega_{lat}s + \omega_{lat}^2} \tag{9}$$

$$\frac{\theta_{des}}{\delta_{lon}} = C_\theta(s) = \frac{\omega_{lon}^2 K_{lon}}{s^2 + 2\zeta_{lon}\omega_{lon}s + \omega_{lon}^2} \tag{10}$$

in

$$\mathbf{C}(s) = \begin{bmatrix} C_w(s) & 0 & 0 & 0 \\ 0 & C_\phi(s) & 0 & 0 \\ 0 & 0 & C_\theta(s) & 0 \\ 0 & 0 & 0 & C_\psi(s) \end{bmatrix}$$

A preliminary evaluation revealed that achievable attitude changes would be too small to meet ADS-33 moderate agility requirements, given the maximum to rated continuous torque ratio of 2 that was selected from the feedback loop analysis. The discussion that follows investigates the effect of torque ratios already considered and accepts limited agility vehicle handling qualities.

Figure 7 shows engine usage for a baseline configuration tuned to provide minimum small- and large-amplitude response characteristics consistent with Level 1 requirements for limited agility. For the roll and pitch ACAH response types these were $\omega_{BW_\phi} = \omega_{BW_\theta} = 2$ rad/s and $\Delta\phi_{max} = \Delta\theta_{max} = 15$ deg. Phase delay values were about 80 ms in both axes. In contrast to the usage elicited for disturbance rejection, response to pilot input induced very different demands on the engines. Pitch response, relying only on four rotors, used the highest torque levels, but torque levels for heave and roll were comparable. Owing likely to the lower response bandwidth (0.5 rad/s), yaw motor usage was comparatively lower (about 30%). With respect to the maximum to rated torque ratio, a ratio of 1.5 still rendered RMS values less than 1.5, but a ratio of 1 was again highly deficient.

Returning our attention to the matter of OLOP prediction, onset frequencies were calculated for torque ratios of 1, 1.5 and 2 (Figure 8). Two approaches were considered based on the closed-loop responses of the rotor speed (Figure 8a) and the motor torque (Figure 8b), respectively. The first approach followed Duda's methodology from Ref. 20, assuming a rotor speed rate limit defined by the maximum rotor acceleration from Eq. 2. The onset frequency was thus determined by the solution of the equation

$$\left| \frac{\Omega}{\delta_{lat}}(j\omega_{onset}) \right| = \frac{\dot{\Omega}_{max}}{\omega_{onset}}$$

7

(a)

(b)
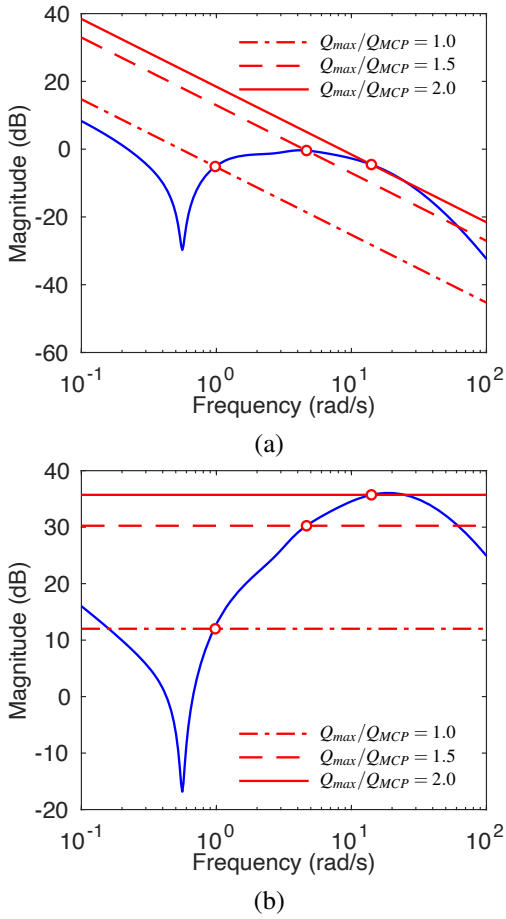
Figure 8. Onset frequencies based on: (a) maximum rotor acceleration and (b) torque limit.

The second approach determines the onset frequency as the frequency where the closed-loop response of the motor torque is equal to the motor torque saturation limit from Eq. 3

$$\left| \frac{\tau_M}{\delta_{lat}}(j\omega_{onset}) \right| = \frac{Q_{upper}}{r_g}$$

It can be seen from Figure 8 that both approaches were equivalent and rendered identical estimates of the onset frequency.

To investigate the broader interconnection between ACAH response type specification and OLOP, command model parameters K_{lat}, ω_{lat}, K_{lon} and ω_{lon} from Eqs. 9 and 10 were swept to span small-amplitude response bandwidth and maximum achievable attitude ranges of 1–3 rad/s and 6.5–25 deg, respectively. Damping ratio parameters were left fixed at $\zeta_{lat} = \zeta_{lon} = 1$ at this time.

Corresponding OLOP loci are shown in Figure 9. Arrows indicate the direction the onset-point amplitude and phase margins change with increasing ACAH response gain or decreasing torque limit. OLOP criteria for limited agility "Level 1" response type specifications (2 rad/s bandwidth and 15 deg achievable attitude) were identified for torque margins consistent with maximum to rated continuous torque ratios of 1, 1.5 and 2.
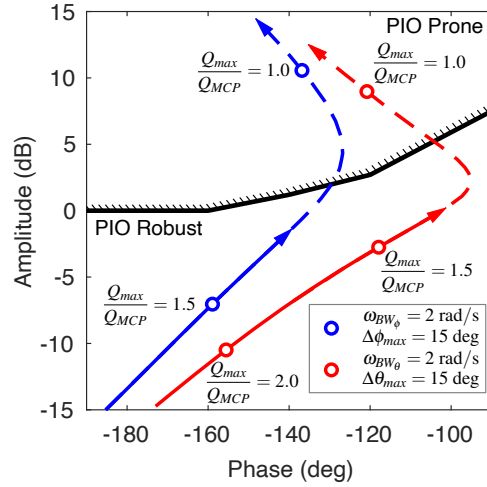
Figure 9. OLOP loci for ACAH response type specifications.

Based on the OLOP criteria, it is evident that limiting the torque to the maximum continuous torque given by the NDARC sizing solution, is unlikely to yield sufficient control power to ensure acceptable handling qualities. Such a configuration would likely be highly prone to PIO and, consequently, be capable only of very limited agility. Doubling the maximum torque limit yielded significantly improved OLOP margins for the baseline design point chosen.

PILOTED EVALUATION

A handling qualities evaluation was conducted in the NASA Ames Vertical Motion Simulator (VMS) to investigate hover and low speed handling qualities of eVTOL aircraft with increased stability and control augmentation under realistic maneuvering requirements (Ref. 24). This section summarizes the key experimental setup considerations from Ref. 24, and presents the results and analysis from a sub-set of the evaluations.

VMS Facility and Conduct of the Experiment

The VMS is a large-amplitude motion-base piloted simulator (Figure 10). The motion system provided very large-amplitude, low-frequency motion cueing to the pilot in all six degrees-of-freedom, but primarily in the vertical (heave) direction (Ref. 25). Interchangeable cabs can be mounted onto the simulator's motion system to implement different seating, display and inceptor arrangements. The Transport-, or T-cab, used has dual pilot seats mounted in the cockpit array. Out-the-Window (OTW) synthetic visual scenes, patterned after Moffett Field, were presented to the pilot via seven collimated image projection "windows" (Figures 11 and 12). The visual imagery was generated using an 8-channel RSi Image Generator. Total processing delay, including the OTW image generation delay, was measured at 72.07 ms before the test. This delay was accounted for in the control law designs
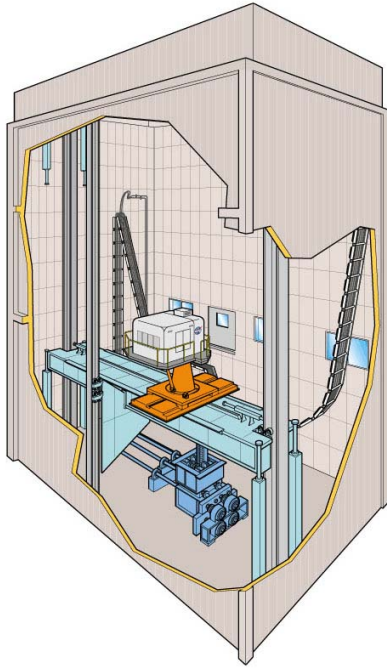
Figure 10. NASA Ames Vertical Motion Simulator (VMS).

(a)   (b)
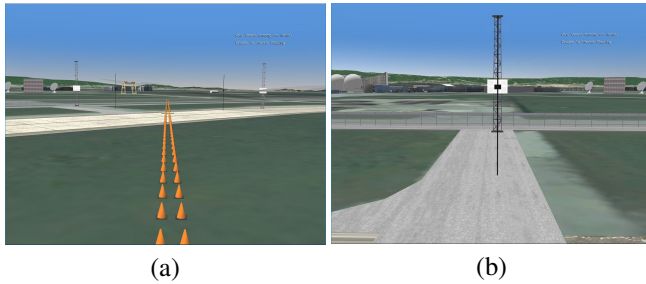
Figure 11. Hover course views from the cockpit: (a) front-right view from the start point, and (b) hover board view from the hover spot.

to render an equivalent phase delay measurement. The Moffett Field database was carefully tailored to contain adequate macro-texture (i.e., large objects and lines on the ground) for the determination of the rotorcraft position and heading with reasonable precision. Aural cueing was provided to the pilot via a WaveTech sound generator and cab-mounted speakers. Rotor noise was emitted to mask external noise from the VMS motion system and enhance the sense of immersion. Rotor airspeed, rotational speed and thrust were used to qualitatively model aural fluctuations. Multiple sources (i.e., rotors) were modeled to enhance the level of realism.

A right hand side stick, a vertically-moving thrust control lever (TCL), and pedal pilot controllers were installed in the cab cockpit for the right hand T-cab seat. Main controller forces, in terms of gradients, breakouts, and friction were provided by a hydraulic McFadden variable force-feel system. Force-displacement relationships for the side stick controller are shown in Figure 13. Note in particular the asymmetry of the lateral force gradient (Figure 13a) required to account for

(a)   (b)

(c)   (d)
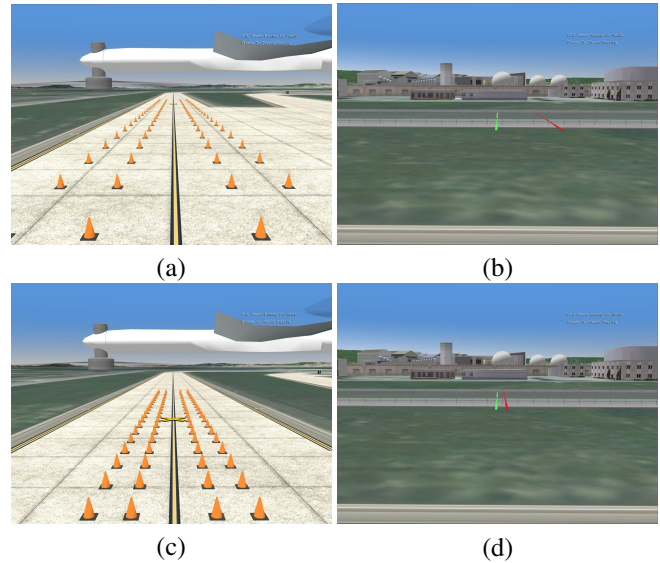
Figure 12. Lateral Reposition course views from the cockpit: (a) right view from the start point (ADS-33), (b) front view from the end point (ADS-33), (c) right view from the start point (UAM), (d) front view from the end point (UAM).

neuromuscular differences in the force exerted between left and right input deflections. Special consideration was given to the dynamic characteristics of the side stick inceptor (Figure 14).

Evaluation tasks Evaluations of the lateral and longitudinal handling qualities were conducted in two Hover Task Elements and two Lateral Reposition Task Elements: the Hover and Lateral Reposition MTEs for Cargo/Utility in Good Visual Environment (GVE) from ADS-33 (Ref. 12), and a Precision Hover and a Lateral Reposition and Hold HQTE patterned after Ref. 14. A comparison of key performance criteria and other maneuver descriptors is summarized in Tables 2 and 3.

Table 2. Hover Task Elements – Performance.

	Hover MTE	Precision Hover HQTE
Performance Criteria		
Horizontal	±3/6 ft	±3/6 ft
Altitude	±2/4 ft	±2/4 ft
Heading	±5/10 deg	±5/10 deg
Deceleration time	±5/8 s	±8/12 s
Maneuver and Test Course Comparison		
Ground speed	6–10 kts	6–10 kts
Reference line	45 deg	45 deg
Altitude	20 ft	20 ft
Maintain stable hover	30 s	30 s

Both Hover evaluation maneuvers utilized the same course, with the only difference between the tasks being the timing
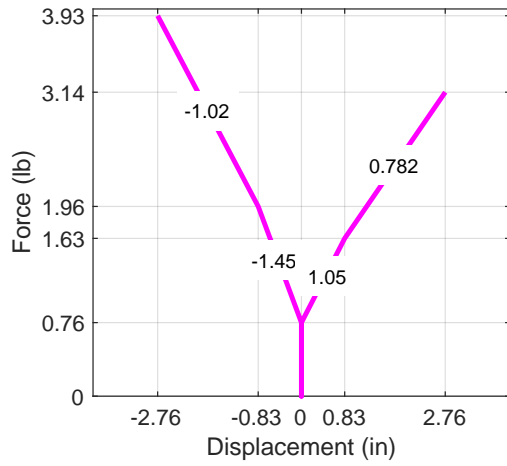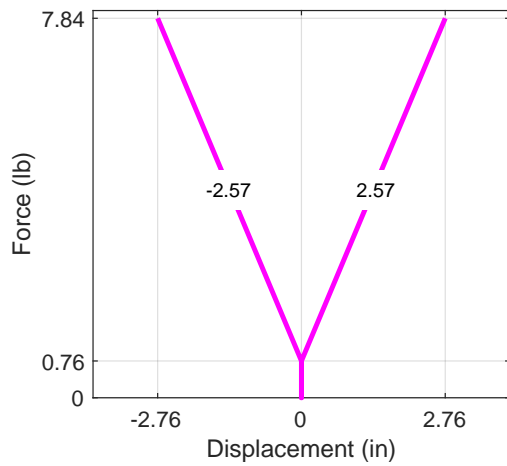
Figure 13. Side stick controller forces: (a) lateral displacement and (b) longitudinal displacement.
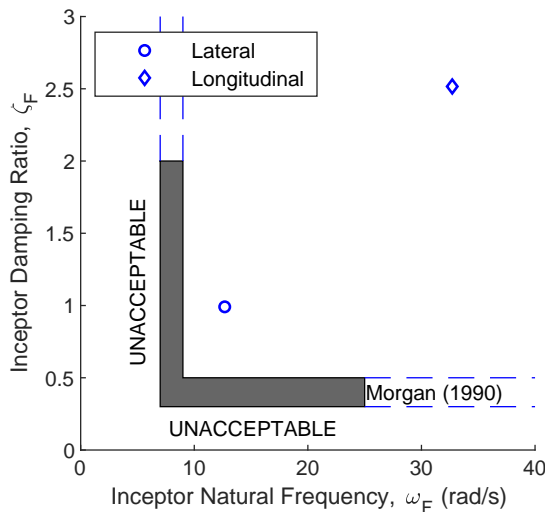
Figure 14. Side stick force-feel dynamic characteristics.

Table 3. Lateral Reposition Task Elements – Performance.

	Lateral Reposition MTE	Lateral Reposition and Hold HQTE
Performance Criteria		
Longitudinal position	±10/20 ft	±5/10 ft
Altitude	±10/15 ft	±5/10 ft
Heading	±10/15 deg	±10/20 deg
Completion time	18/22 s	—
Ground speed	—	10±2/4 kts
Maneuver and Test Course Comparison		
Initial altitude	40 ft	20 ft
Course length	400 ft	120 ft
Endpoint margins	±10 ft	±5 ft
Maximum overshoot	—	5 ft
Maintain stable hover	—	5 s

required to attain a stabilized hover after initiation of the deceleration into the target hover area. The Lateral Reposition maneuvers, while similar in general construct, differed in a number of ways. The Lateral Reposition and Hold HQTE emphasized higher precision and lower aggressiveness, necessitating adjustments to the test course. Lines of cones marking the desired and adequate longitudinal track were moved in closer to the center line (Figures 12a and 12c) and the maneuver was flown at a lower altitude. Instead of targeting a completion time, the Lateral Reposition and Hold HQTE required the pilot to achieve a target speed of 8–12 kts. For experimental expediency the course was shortened to 120 ft. One final modification, not affecting the course, was the addition of a requirement to hold a stable hover for 5 seconds within designated lateral position tolerances before termination of the maneuver.

Turbulence model The rotorcraft response with wind and turbulence was simulated using a modified Dryden model for ease of implementation. The Dryden model can be ill-suited for rotorcraft simulation, especially at slow airspeed, primarily due to its underlying assumption that the vehicle's airspeed is large compared to the turbulent perturbations (Ref. 26). To make the Dryden model more suitable to this application, the Dryden transfer functions were interpreted to produce disturbances aligned with vehicles aerodynamic frame with mean atmospheric wind, as if the vehicle were flying through a static atmosphere. The turbulent disturbance was then transformed to the body-frame of the rotorcraft and subtracted from the ground-relative state before using it to compute aerodynamic related forces and moments according to the vehicle's math model. The modified Dryden model also used a tunable minimum airspeed parameter (independent of the simulated mean-wind) to keep the turbulent perturbation bandwidths within acceptable tolerances for the simulation as judged by a project pilot. The Dryden parameters used for the study were 60 kts minimum airspeed, 60 ft span, and turbulence magnitude settings for a mean wind speed of 15 kts in accordance with the low altitude Dryden model specification (Ref. 27). Table 4

shows the RMS airspeed and rotational rate perturbations generated by the Dryden model in the aerodynamic frame with x-axis pointing in the direction of the mean-wind, y-axis to the right, horizontal to the ground, and z-axis completing the right-handed orthogonal system.

Table 4. Modified Dryden Model: RMS Perturbations.

Altitude	σ_u	σ_v	σ_w	σ_p	σ_q	σ_r
ft		ft/s			deg/s	
20	2.75	2.75	1.42	1.87	0.99	1.71

Experimental Configurations

Three NASA-designed eVTOL concept vehicles (Refs. 2, 10) were studied, including the variable-collective Quadrotor, the variable-RPM Hexacopter, and the Lift+Cruise vehicle with eight variable-RPM lifting rotors (Figure 15). Flight dynamics models strictly represented the coupled rotor-airframe dynamics. Rotor aerodynamics were based on BEMT, using 3-state dynamic inflow unsteady wake models, and included rotor flapping dynamics and rotational degrees of freedom. Airframe and rotor sectional aerodynamics were based on look-up table aerodynamics, and rotor-to-rotor and rotor-to-airframe aerodynamic interactions were not modeled. Key vehicle characteristics from NDARC are summarized in Table 5. The Quadrotor is designed with an interconnected drivetrain that connects all rotors to the engine group, hence the large drive torque limit for the Quadrotor. For clarity, it does not use individual direct-drive or RPM control.

Flight Control System A common control system architecture, shown in Figure 16, was used to enable the following augmented control modes: Attitude Command-Attitude Hold (ACAH), Rate Command-Attitude Hold (RCAH), and Translational Rate Command (TRC) for roll/lateral and pitch/longitudinal control; Rate Command-Direction Hold (RCDH) for directional control; and Rate Command-Height Hold (RCHH) for vertical control. Each vehicle was equipped with a linear quadratic integral (LQI) feedback control system with integral action applied to the roll, pitch, yaw, and heave axes for command tracking and feedback stabilization. The LQI feedback gains were tuned to attain minimum disturbance rejection bandwidth (DRB) and disturbance rejection peak (DRP) metrics per proposed ADS-33F standards (Ref. 12). Electric powertrain models were sized for each configuration to enforce realistic saturation and rate limits. During the gain tuning process, it was observed that increases in DRB required higher amplitude motor torque responses; therefore, the disturbance rejection responses were placed near the Level 1 boundary to mitigate loss of control (LOC) behavior due to control saturation.

Command model filters were placed upstream of the feedback controller to target proposed ADS-33F standards (Ref. 12) pertaining to small-amplitude responses in the low-speed and hover regime, as well as TRC metrics from Franklin and

Table 5. Experimental Aircraft Model Characteristics.

Characteristic	Quad	Hex	LpC
Design Gross Weight (lb)	6,427	6,510	6,651
Payload (lb)	1,200	1,200	1,200
Empty Weight (lb)	5,216	5,299	5,180
Capacity (Pax + Crew)	6	6	6
Number of Rotors	4	6	8
Design Disk Loading (lb/ft^2)	3	3	10.6^a
Number of Blades	3	3	2
Blade Pitch@75% (deg)	–	11.7	16.5
Rotor Radius (ft)	13.1	10.7	5.0^a
Solidity, thrust-weighted	0.056	0.056	0.176
Design Tip Speed (ft/s)	550	550	550
Design Rotor Speed (rad/s)	42	51.3	110
Flapping Frequency (1/rev)	1.03	1.03	1.25
Lock Number	5.16	4.61	1.46
Moments of Inertia (slug ft^2)			
I_{xx}	15,540	8,385	6,893
I_{yy}	16,963	18,866	4,500
I_{zz}	20,525	23,291	9,611
I_{xy}	0	0	0
I_{yz}	0	0	0
I_{xz}	0	0	0
Rotor Inertia (slug ft^2)	265.8	109.2	13.5
Propulsion Group	Central	Direct	Direct
Number of Motors	4	6	8
Engine			
– SLS Power per Motor (hp)	111.5	87.0	123.0
– Specification Speed (rpm)	8,000	8,000	8,000
– Shaft Power Limit (hp)	319.9	211.7	262.2
Drive Torque Limit (ft-lb)	8,320	1,136	656
Battery Capacity (MJ)	1,316	1,449	1,215

^{a}The Lift+Cruise design constrains rotor size

Stortz (Ref. 28) and Malpica et al. (Ref. 29). Various sets of command model frequencies and damping ratios were selected to explore the criteria's design space and are shown in Figures 17 and 18. Here, the designations refer to aircraft (Q for Quadrotor, H for Hexacopter and L for Lift+Cruise), command model (α for Level 1 and ζ for Level 2) and augmentation (A for ACAH and T for TRC). Notional Level 1 handling qualities boundaries in Figure 18 are from Ref. 29. The command model parameters for the collective-controlled Quadrotor were selected to have a large margin within the Level 1 small-amplitude response region. The Quadrotor was intended to act as the experiment control configuration for comparison to the other vehicles. The Quadrotor utilized collective pitch actuators, also depicted in Figure 16, which enabled much higher bandwidth responses in comparison to the variable-RPM configurations. There were two sets of command model parameters for the variable-RPM Hexacopter. The first set placed the small-amplitude responses within the Level 1 region and the maximum achievable bandwidth was limited by the control margin imposed by torque saturation limits. The second set of Hexacopter command model parameters was selected to place the response in the Level 2 region.
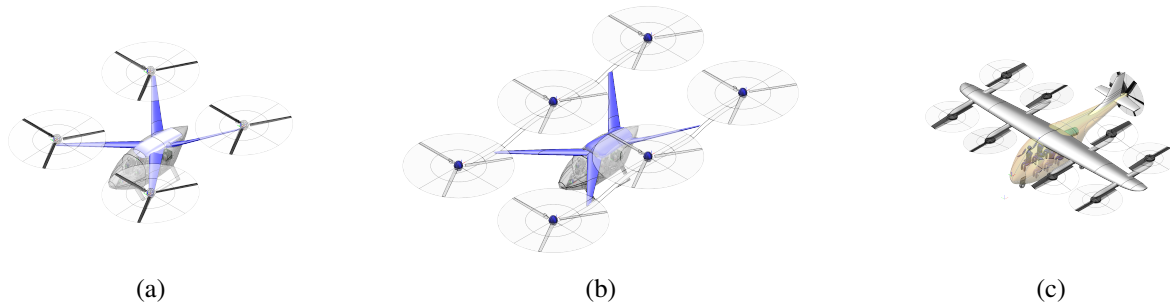
Figure 15. Renderings of the concept designs: (a) Quadrotor, (b) Hexacopter, and (c) Lift+Cruise.
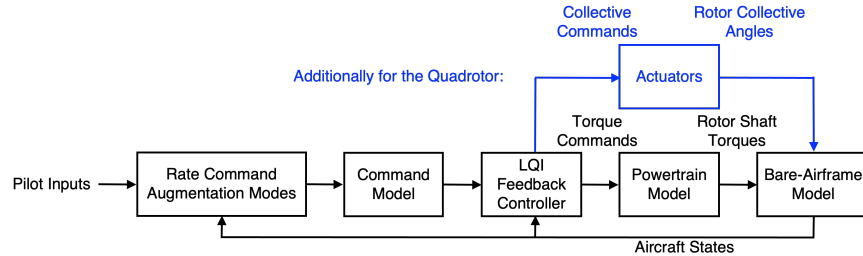
Figure 16. Common LQI flight control system architecture.

This was done to explore the effect of degraded bandwidth and phase delay on the handling qualities. The Lift+Cruise command model parameters were selected to place the response in the Level 1 region and their tuning was also driven by motor saturation limits. This vehicle was also used to study the impact of propulsion failures on handling qualities, and this objective impacted its control system design (Ref. 30).

The flight control gains were increased during the tuning process to account for the visual system time delay. This was needed to provide true measures of the phase delay in Figures 17 and 18. Unfortunately, this had the unintended effect of artificially increasing the engine usage. To compensate, torque commands going into the motor controllers were proportionally scaled down, and, subsequently, engine output torques were scaled back up so that rotor shafts would see the torques necessary to match the dynamics of Figures 17 and 18. While successful in matching peak torques, the full consequences of this approach are not yet fully understood.

Powertrain Model

Model development A realistic powertrain model was desired to estimate the influence of the powertrain and parameters sized for the powertrain on handling qualities. Central to the powertrain architecture was the Permanent Magnet Synchronous Motor (PMSM). The PMSM has advantages over other electric motors in efficiency, power density, size, and weight (Ref. 31). A PMSM has permanent magnets in the motor rotor that create a constant magnetic field. Torque is generated by controlled multiphase electrical current flowing through the motor stator windings/coils producing a rotating magnetic field that interacts with the motor rotor permanent magnets.

The PMSM and its system requirements are central to the powertrain architecture. The powertrain system architecture is depicted interfaced with the pilot, vehicle and flight controller for VMS testing in Figure 19. The flight controller interprets pilot commands into motor torque commands. The motor torque commands are resolved within the flight controller for both cases of blade pitch command or RPM command flight controllers.

Motor torque commands in Figure 19 are interpreted by motor controllers into current commands, which are transformed into pulse width modulation (PWM) commands after passing through the motor control laws. The motor control laws implement field-oriented control using a maximum torque per amp (MTPA) control strategy (Ref. 31). The MTPA controller is augmented for over-rated motor conditions with a flux weakening controller. The flux weakening controller is passively implemented so as to not interfere with the MTPA controller when the motor is operating up to its rated speed and torque condition (Ref. 32). The flux weakening controller prevents inverter saturation; this is necessary to avoid open-loop motor dynamics. The PMSM current dynamics are augmented with nonlinear decoupling and feedforward back-electromagnetic field (back-EMF) control (Ref. 33). The additional nonlinear control laws are meant to linearize the current dynamics by approximately canceling strong nonlinear coupling terms in the PMSM equations of motion.

During flight, the motor temperature may increase. As the motor temperature increases, the stator resistance increases, while the back-EMF constant tends to decrease. A thermal
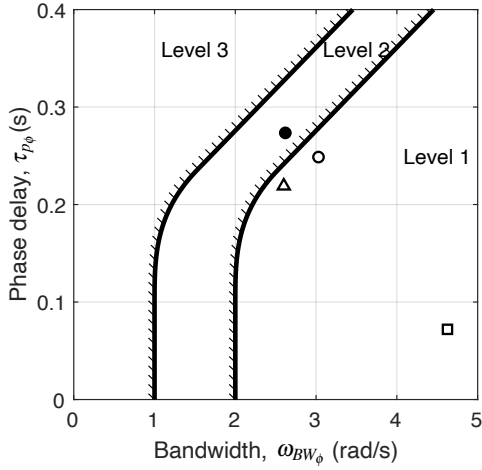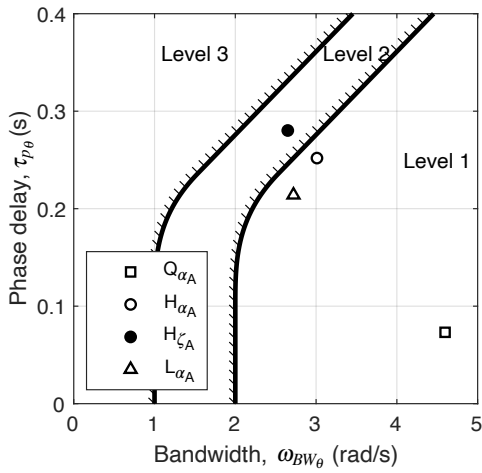
Figure 17. ACAH configurations: (a) roll and (b) pitch.

Figure 18. TRC configurations: (a) sway and (b) surge.

model was derived in (Ref. 34) to capture these potentially significant impacts on the powertrain performance. The thermal model includes heat loss from hysteresis, resistance, and friction. The thermal model approximates the stator case, stator winding, and the motor rotor as lumped masses with an assumed water glycol coolant type and fixed coolant temperature.

The PMSM stator winding coils are powered by an inverter and battery. The voltage commands to the inverter from the motor controller are converted to PWM signals. The output voltages of the inverter assume space vector pulse width modulation (SVPWM) is in place. For computational efficiency, transistor switching was assumed to be instantaneous. To account for heat efficiency losses in the inverter, a hard-coded 1% increase in power draw from the motor on the battery pack was assumed.

The battery pack serves as the sole DC-link to the inverter. The battery pack, one per inverter, was modeled as a parallel arrangement of strings of 18650 lithium-ion polymer (LiPo) batteries. The dynamics of each 18650 battery were modeled with empirical equations (Ref. 35) with a correction to

modernize cell internal resistance. As the battery heats up, the voltage of the battery tends to increase, but operations at higher temperatures degrades battery cell life. A lumped mass approximation was used to generate a thermal model (Ref. 36) of each battery cell surface assuming air cooling. Every cell of the battery is assumed to behave identically to all other cells in terms of current draw, voltage drop or temperature change for computational efficiency.

Parameter sizing The motor torque coefficient and back-EMF constant were sized assuming a known motor rated continuous power and speed from NDARC. The motor resistance was sized assuming a known electrical efficiency which can be used to relate the electrical power input of the PMSM to its output mechanical power. Stator resistance and back-EMF constant affects the motor stator voltage achieved at the motor's rated condition.

The battery packs series and parallel configurations were sized to exceed the motor's rated DC voltage for the duration of the mission. This meant that choices of the DC rating of the motor had a significant impact on the longevity of the battery.
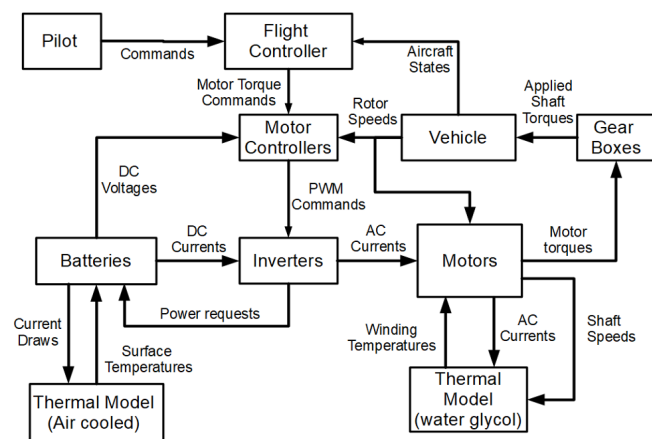
Figure 19. Powertrain system architecture.

The inverters were not directly current limited since the motor torque and therefore current was already limited.

The motor thermal parameters were sized using a scaling parameter on experimental thermal data taken from Ref. 34. The scaling parameter assumed that the thermal resistance of each lumped mass scales linearly with increasing rated continuous power of the motor.

Torque and voltage limits The motor torque commands from the flight controller were limited by saturating the motor torque command internal to the motor controller. The torque limits assume intermittent torque was allowable up to twice the rated continuous torque of the motor. The duration that an intermittent torque command is allowable is governed by the winding temperature of the motor.

The stator resistance and back-EMF constant affect when flux weakening control is required to prevent inverter saturation. Another important contributor to flux weakening control engagement is battery voltage. When flux weakening control is engaged, AC current is adjusted to generate more magnetic losses, having the effect of limiting the motor torque output capability below the rated continuous torque.

The relevant powertrain sizing parameters and limitations are captured in Table 6. Both the Quadrotor and the Hexacopter powertrains were sized to maximize torque potential, using 8,000 rpm as a reference rated speed and a known rated continuous power rating. The Lift+Cruise powertrain sizing instead maximized its rated speed. This was made necessary to avoid hitting voltage limits, which seriously limited the control authority of the vehicle, as determined during the simulation development.

Modeling simplifications The aforementioned powertrain model is difficult to integrate into control design, due to computational requirements as well as complexity. Simplifications were made to the complex powertrain architecture in Figure 19. The battery voltage was assumed to be constant. The temperature of the motor was assumed to be fixed. Only the torque axis of the current equations of the PMSM were

Table 6. Powertrain Parameters and Limits.

Characteristic	Quad	Hex	LpC
Rated Continuous Power (kW)	83.1	64.9	91.7
Rated Continuous Torque (Nm)	99.2	77.4	98.2
Peak Torque (Nm)	198.5	154.9	196.5
Rated Continuous Speed (rpm)	8,000	8,000	8,900
Stator Current Limit (A_{pk})	398.8	311.2	440.3
Current Rate Limit (kA_{pk}/s)	3.01	3.01	3.36
Battery Voltage 100% SOC (V)	700	700	700
Stator Voltage Limit (V_{pk})	350	350	350
Battery Capacity (MJ)	1,316	1,449	1,215
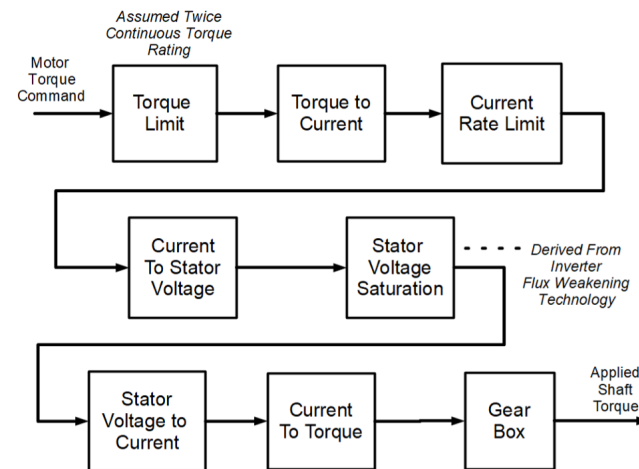
Figure 20. Simplified powertrain model.

modeled. These simplifications resulted in an architecture as shown in Figure 20.

The theoretical performance of the SVPWM inverter with flux weakening technology was used to determine the stator voltage saturation limit. The torque limit of the motor command was maintained at twice the continuous torque limit. A current rate limit which is identical in both complex and simple powertrain models would typically be used to protect motor controller circuitry.

Robustness to powertrain limiting Given the various limits in the powertrain, it was of interest to determine the most critical in terms of their potential for triggering Category II or III PIO. The onset frequencies for an experimental Hexacopter configuration with ACAH control augmentation (H_{α_A}), for example, are shown in Figures 21–23 for key limits from Table 6. It was apparent that torque saturation (Figure 21), with an onset frequency of about 2.1 rad/s, was the critical limit for the specific powertrain configuration considered. The current rate limit (Figure 22) rendered an onset frequency closer to 6.6 rad/s, and the stator voltage limit (Figure 23) was not reachable with a maximum input deflection.

Roll OLOP criteria for the Hexacopter and the Lift+Cruise ACAH configurations (H_{α_A} and L_{α_A}), calculated at the torque limit onset frequencies, are shown in Figure 24. The LQI state feedback controller loops were broken, one at a time,
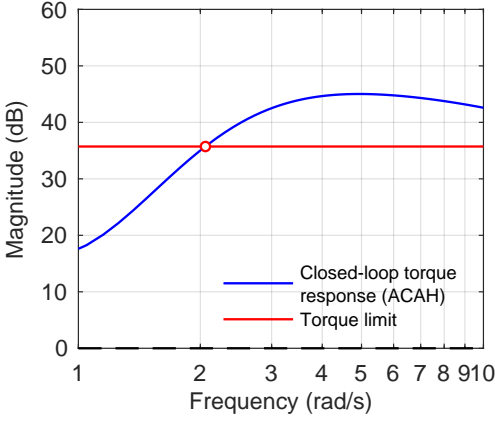
Figure 21. Motor torque limit onset (Hexacopter motor 1, ACAH).
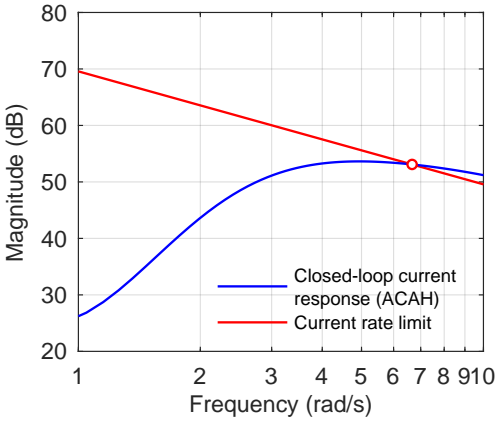
Figure 22. Current rate limit onset (Hexacopter motor 1, ACAH).
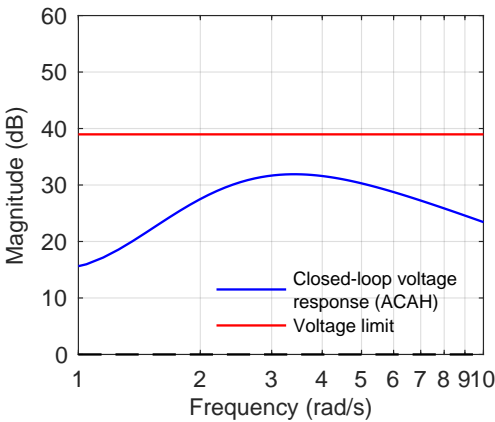
Figure 23. Stator voltage limit onset (Hexacopter motor 1, ACAH).
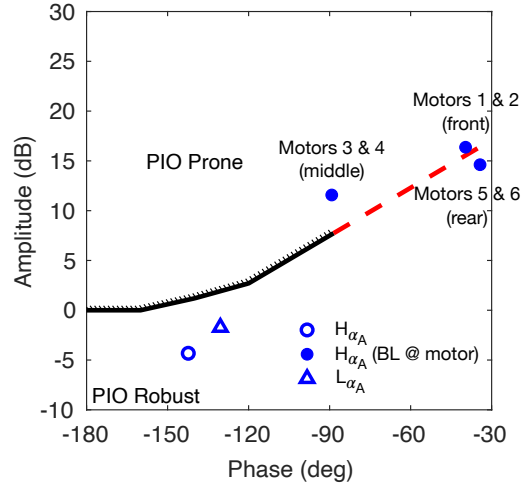
Figure 24. OLOP for ACAH configurations (roll).

at various points (at the torque command signals to the motor controllers, at the error signal and upstream of the control mixer) to determine the worst case OLOP margins. Breaking the loop at the error signal, ϕ_e, resulted in OLOP margins consistent with the preliminary CONDUIT analysis. These margins would seem to predict fairly PIO robust configurations.

However, breaking the loop at the individual torque command inputs to the motor controllers, as fundamentally suggested by Duda (Ref. 20), resulted in OLOP gain and phase values ranging from 12 to 17 dB and -90 to -30 deg, respectively. Of these, breaking the loop at motors 3 and 4 would appear to indicate a strong potential for PIO being triggered by saturation of the motor torques. The remaining OLOP criteria were characterized by much smaller phase values. It is unclear without further analysis whether jump phenomena originating from the activation of torque saturation limits within these loops would be conducive to PIO behavior. A hypothetical extension of the boundary from the existing guidance was plotted (in dashed lines) for reference purposes only.

Results

Cooper-Harper Handling Qualities Ratings (HQRs, Ref. 37) from the piloted evaluation are summarized in Figure 25. Configurations in Figure 25 are ordered along the principal axis by order of increasing control augmentation, defined both by increased response type stability (TRC over ACAH) and higher response bandwidth. From this perspective, configuration H_{ζ_A} represented the lowest level of augmentation, and configuration Q_{α_T} the highest (refer again to Figures 17 and 18 for the specific values). Note that ratings of 4.5 were allowed as a compromise between desired performance being attained, but requiring considerable pilot compensation. The following are the key observations from the assigned HQR values.

Effect of augmentation Increasing levels of augmentation broadly resulted in improved handling qualities, which was to
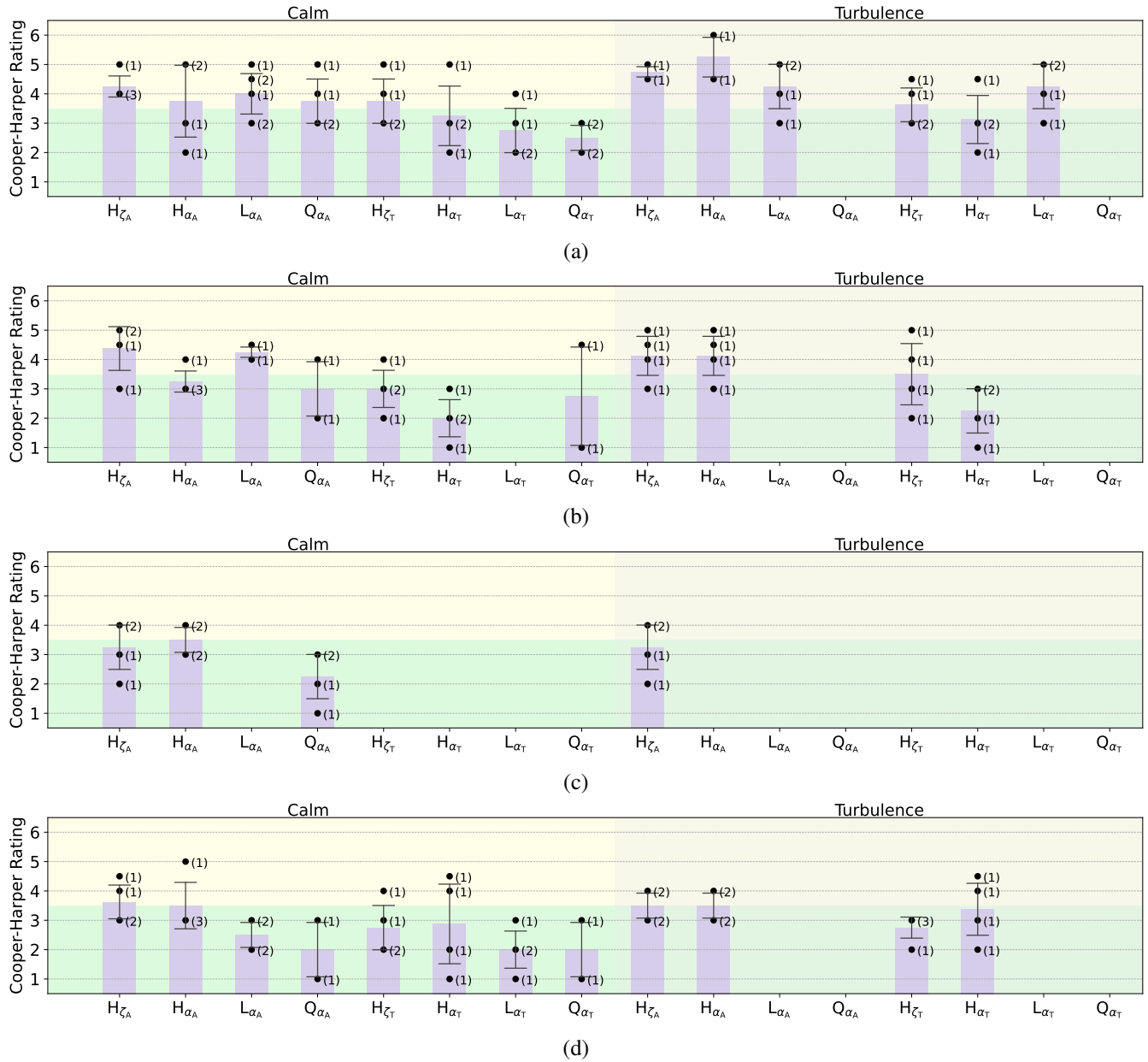
Figure 25. Handling Qualities Ratings (number of pilots in parenthesis): (a) Hover MTE, (b) Precision Hover HQTE, (c) Lateral Reposition MTE, and (d) Lateral Reposition and Hold HQTE.

16

be expected. ACAH alone, however, did not result in Level 1 handling qualities from all evaluators in either of the Hover tasks (Figures 25a and 25b). This included the Quadrotor control case, Q_{α_A}. Evaluations in the Lateral Reposition tasks (Figures 25c and 25d) resulted in slightly lower (improved) HQR values, compared to the Hover tasks, with a significant number of ratings in Level 1 for both ACAH and TRC response types. With a few outliers, which warrant specific examination, TRC with higher response bandwidth (lower time constant) achieved Level 1 handling qualities more consistently, particularly in calm air conditions.

Examination of the "outlier" Level 2 ratings revealed that most of the ratings were from the same pilot, which makes these useful datapoints, as it was indicative of something unique about this pilot's control technique or appreciation of the vehicle deficiencies. This particular pilot provided the Level 2 rating for H_{α_T} in the Hover MTE and one of the ratings in the Lateral Reposition and Hold HQTE; and the Level 2 rating for configuration Q_{α_T} in the Precision Hover HQTE. This pilot did not evaluate L_{α_T}, but examining evaluation comments for this configuration revealed similar objections from the pilot that rated it Level 2. The same was true from the evaluation of the second pilot that rated configuration H_{α_T} in the Lateral Reposition and Hold HQTE as Level 2.

In general, configurations H_{α_T}, L_{α_T} and Q_{α_T} exhibited significant jerkiness, especially when making small input corrections around the detent, and some tendencies to over control or initiate unintended motion. Pilots described a "very responsive" or "abrupt" vehicle response. Configuration Q_{α_T} in particular was penalized for the "deficient ride quality," even though desired performance was achieved and not in question. Configuration Q_{α_T} differed from the other two primarily in the severity of the response characteristics and deserves some further attention: a "very objectionable" response in roll was characterized by the pilot as "ratcheting". This was triggered whenever the pilot had to make small inputs around the detent, specifically as pilot "attempted to reduce aggressiveness" during the deceleration. While the high responsiveness of the system correlated with response bandwidth, evaluation comments pointed to a sub-optimal response sensitivity to inceptor input.

The lateral axis average control response sensitivity in the VMS was about 10.8 ft/s/lb, or 10.9 ft/s/in. In both instances, this was higher than what is recommended in ADS-33, which is consistent with the pilot assessments. Configurations H_{α_T}, L_{α_T} and Q_{α_T}, with a TRC bandwidth of 0.33–0.35 rad/s, all enabled precise position control within the task-prescribed desired requirements, however. Configuration H_{ζ_T}, with a bandwidth of 0.16 rad/s, did not universally afford the precision to execute tasks within desired performance levels, without increasing the workload. Generally, pilots confirmed they needed to be "more deliberate with putting in the opposite stick" or "had to stay more involved with the deceleration" in order to capture targets within the desired position tolerances or times. Despite the controller sensitivity deficiencies, which led to the aforementioned issues, the 0.33 rad/s TRC bandwidth appeared conducive to Level 1 handling qualities.

Task aggressiveness With a few exceptions, the Hover MTE tended to elicit slightly higher ratings (Figure 25a) compared to those from the Precision Hover HQTE (Figure 25b). Configuration Q_{α_T}, already discussed above, was the only one that opposed this trend. However, it should be remembered that specific reasons for the rating were given precisely in response to an objectionable roll axis motion ("ratchet") that resulted from the pilot's attempts to reduce his aggressiveness. This caused the pilot to require smaller inputs around detent, where the input response sensitivity was likely too high, versus larger inputs. Again, this pointed to a sub-optimal mechanization of the commanded vehicle response per unit of inceptor displacement, rather than a deficiency in the response bandwidth of the TRC control law.

Interestingly, though, this deficiency was uncovered because of the pilot's attempt to match the lower task aggression required by the Precision Hover HQTE. The task could have been flown more aggressively and the pilot could have well-exceeded the minimum desired performance without eliciting this objectionable ride quality characteristic. More generally, it was the objectionably "jerky" response that was triggered by the increased task aggressiveness of the Hover MTE that was described by the pilots as the cause for the higher ratings. Again, though, it is worthwhile pointing out that it was the over-responsiveness of the vehicle that was objected to, and hence the ride comfort, and not a lack of control authority.

The Lateral Reposition MTE is by definition intended to evaluate handling qualities of a configuration under moderate agility maneuvering requirements. Only ACAH configurations were evaluated in this task (Figures 25c). Comparatively, the Lateral Reposition and Hold HQTE required smaller maneuver attitude changes, but higher precision. This trade-off appeared finely balanced, judging by the numerically-similar ratings for the ACAH configurations tested (Figures 25c and 25d). The two tasks were sufficiently differentiable, however, to expose different characteristics of the aircraft, or to expose them with varying severity: agility required by the Lateral Reposition MTE uncovered a HQ cliff in a way the Lateral Reposition and Hold HQTE did not. Instances of loss of control will be examined in the next section below, but were caused by the activation of limits in the drivetrain. The Lateral Reposition and Hold HQTE, without causing the loss of the aircraft, did however cause the aircraft to exhibit characteristics that would hint at the potential for loss of control. In particular, the Hexacopter ACAH and TRC configurations, H_{α_A} and H_{α_T} respectively, exhibited an oscillatory "ratcheting" behavior that was characterized by the pilots as "typical of a limiting behavior". These deficiencies were the reason for Level 2 ratings being assigned to both these configurations.

The roll ratchet is a type of PIO behavior typically associated with the bio-mechanical coupling of the inceptor and pilot arm/limb, and is usually not severe. Time histories from the three evaluation runs of configuration H_{α_A} by one of the pilots that indicated the presence of a roll ratchet behavior are shown in Figure 26. The delay between the pilot command and the roll response is evident in all three runs. In-

(a)

(b)

(c)
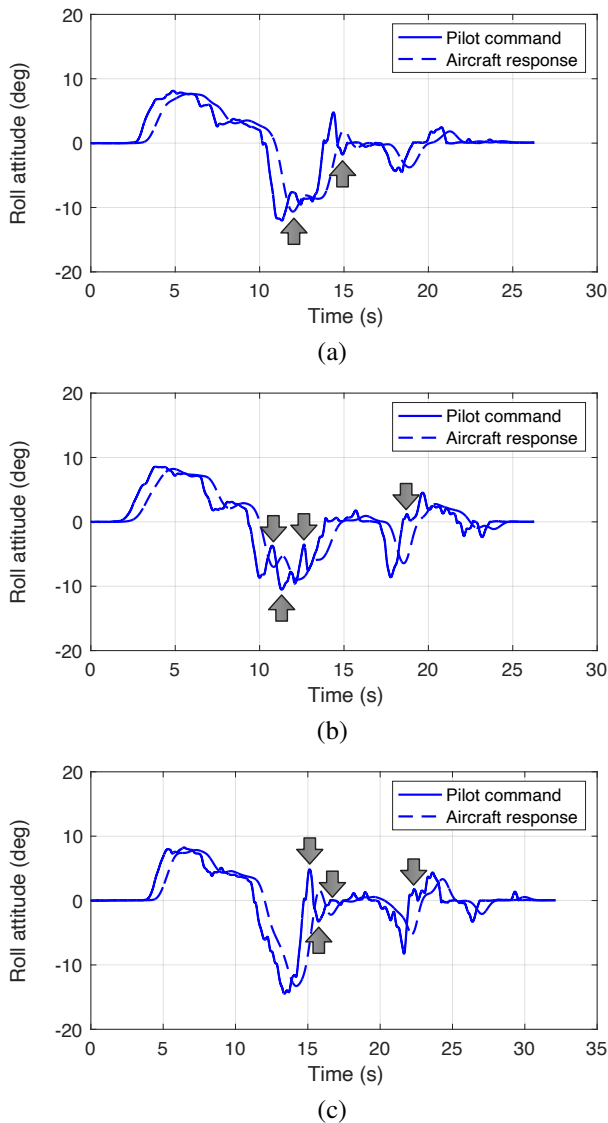
Figure 26. Illustration of PIO: (a) run 1, (b) run 2, and (c) run 3.

stances where the pilot input and the vehicle response can be judged to be 180 deg out-of-phase are indicated on the time history traces, are not severe, and ranged in frequency from 0.7–1 Hz. These frequencies are likely too low for this PIO to be considered roll ratchet. Rather, this frequency seemed more closely aligned with the ACAH small-amplitude response phase crossover, and incidentally, the rotor speed control crossover. It should also be remembered that H_{α_A} has significant phase delay (about 250 ms), so PIO tendencies are not unexpected. In any case, it was confirmed that saturation or rate limits in the powertrain were not activated at any moment during these runs, so the out of phase behavior could not be attributed to these types of nonlinearities. While it has not been positively confirmed that these pilot-vehicle oscillations were caused by the coupling of the arm and inceptor dynamics, it is understandable how the pilot could have interpreted them as such.

Between the four tasks, turbulence had the strongest effect on the ratings for the Hover tasks (Figures 25a and 25b). Effect of turbulence on ratings from the Lateral Reposition tasks (Figures 25c and 25d) was minimal. For these highly-augmented control laws, turbulence was not sufficiently strong to affect the task performance. Pilots could and did accept the turbulence-induced aircraft motion without suffering a performance penalty. Effect of turbulence in the Hover tasks was not uniform across configurations, however, with H_{α_A} and L_{α_T} being the most susceptible.

Examination of the evaluations from the two pilots who rated the H_{α_A} case in both calm air and turbulence revealed widely different outcomes depending on the control strategy. For one pilot, the handling qualities degraded from an HQR 3 in calm air, to an HQR 6 in turbulence. For the second, the change was very minor, and actually beneficial, from an HQR 5 in calm air to an HQR 4.5 in turbulence.

The first pilot reported that "station-keeping [in turbulence] was [made] more difficult because of motor rates," with a "jerky response to inceptor [input]," "PIO tendencies," and unpredictable response. All of these point to an increased activity by the pilot trying to reject the disturbances. In contrast, the second pilot chose to back out of the loop to "allow aircraft to counter most turbulence with some pilot input," while "trying to ignore bump from the turbulence." Interestingly, in calm air the situation was inverted, with the second pilot operating at a level of aggressiveness that uncovered the aircraft's "tendency to over control," with an "abrupt and delayed" response that exhibited "[a] lot of jerkiness."

Loss of control Figure 27a shows three different attempts by the same pilot to perform the Lateral Reposition MTE with the Hexacopter in ACAH (H_{α_A}). This task required the pilot to accelerate laterally from hover to 20–25 kts and then quickly stop at a designated point and re-stabilize. On the first run (in blue), the pilot performed a very aggressive control reversal to decelerate, leading to a loss of control (LOC). The cause of the LOC was powertrain torque limiting, which in turn led to motor speed rate limiting, shown in Figure 27b as a classical sawtooth-shaped response. On his second attempt (in black), the pilot was much less aggressive and did not encounter rate limiting. Two attempts later (magenta), the pilot increased his aggressiveness and again encountered the rate limiting but was able to maintain control and complete the task.

These results illustrate the importance of including high-fidelity model characteristics when evaluating pilot handling qualities, of designing tasks that encourage the pilot to explore regions of the operational envelope that might contain a sudden deterioration of handling qualities, and in seeking evaluations from a large and diverse group of pilots. Not every pilot will uncover the same hidden issues.

The positive confirmation of Category II PIO occurring during aggressive maneuvering gave credence to the OLOP prediction from Figure 24, based on the loops being broken at the motor torque command inputs. Breaking the loop for the
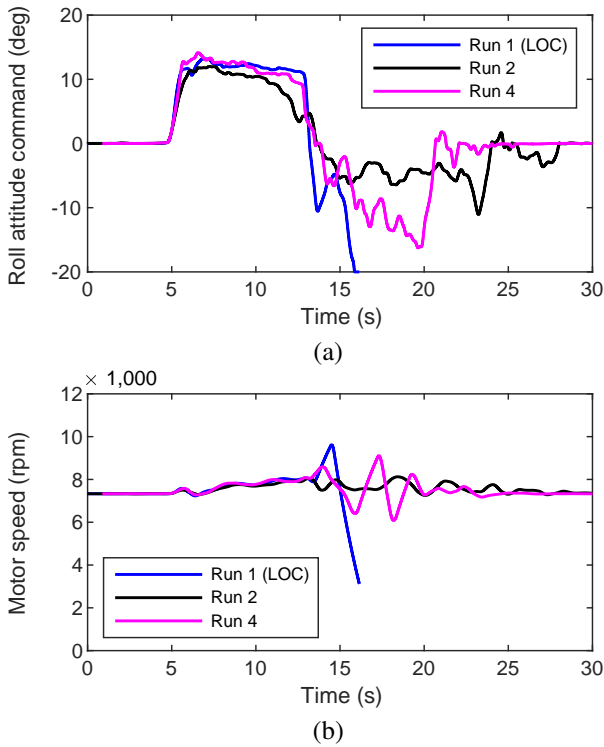
Figure 27. Illustration of loss of control: (a) roll command and (b) motor #2 speed.

OLOP criteria at the error signal alone did not accurately predict the occurrence of PIO.

Engine usage Overall torque magnitudes required during typical maneuvering flight are one of the key metrics for engine usage characterization. The rated continuous torque was found to be frequently exceeded during the execution of the evaluation maneuvers for both ACAH and TRC response types. Figure 28 shows, for example, the frequency of individual torque exceedance events for the Hexacopter from all Lateral Reposition runs. On average, the continuous torque threshold (Q_{MCP}) was exceeded about 16.4 times per run. The $1.5Q_{MCP}$ threshold was exceeded in about 19% of these instances (Figure 28b), and less than 5% of events reached the $2Q_{MCP}$ saturation limit (Figure 28c). The cumulative average time per evaluation run spent at, or in exceedance of, the given torque thresholds for the two response types was comparable: 56% (Q_{MCP}), 7.0% ($1.5Q_{MCP}$) and 2.1% ($2Q_{MCP}$) for ACAH, and 49% (Q_{MCP}), 6.3% ($1.5Q_{MCP}$) and 1.8% ($2Q_{MCP}$) for TRC. In this instance, neither of the control laws elicited significantly different usage.

The second aspect of the engine usage to consider are its dynamic characteristics. The pulsing nature of the torque demands on the motor is illustrated in Figure 28: approximately 72% of the continuous torque exceedances were less than 1 s long and 94% were shorter than 2 s. Control of the aircraft with ACAH appeared to require about twice as many short duration (less than 0.5 s) pulses, compared to TRC. This was likely caused by the pilot needing to provide additional stabi-
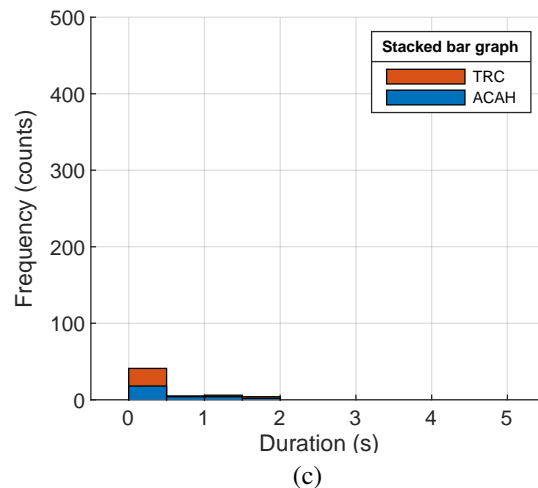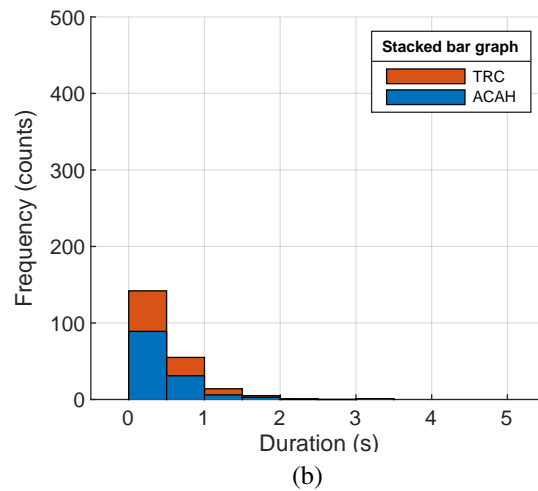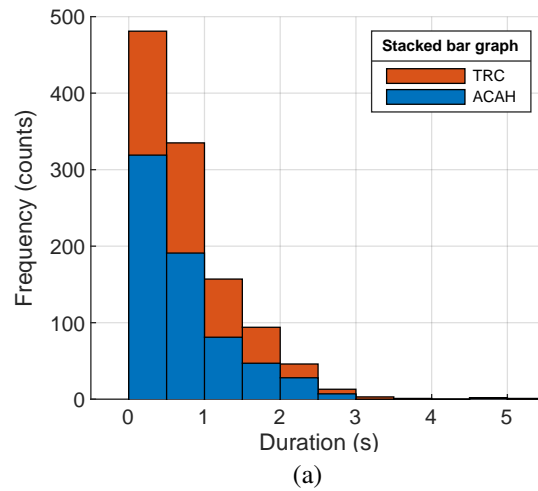
Figure 28. Hexacopter motor torque threshold exceedances (all engines) during Lateral Reposition tasks: (a) $\boldsymbol{Q_{MCP}}$, (b) $\boldsymbol{1.5Q_{MCP}}$, and (c) $\boldsymbol{2Q_{MCP}}$.

lization, and doing so in a less smooth manner. There were 36 runs with ACAH and 33 with TRC, so the counts per response type were comparable.

Overall, maximum typical duration of the torque command pulses to the motor controller were about 3 s, although a few instances of longer duration were evidenced. The maximum torque limit of $2Q_{MCP}$ was generally sufficient, also, and only infrequently reached, for the agility that was required of the vehicles.

CONCLUSIONS

The following conclusions can be established based on results presented above:

1. Increased control augmentation in the form of Translational Rate Command (TRC), with a bandwidth of 0.33 rad/s can provide improved handling qualities over Attitude Command-Attitude Hold (ACAH) in high precision tasks such as the hover maneuvers evaluated, where agility requirements were low.

2. Level 1 hover and low speed handling qualities are feasible for eVTOL aircraft (capable of payloads up to 1,200 lb) using RPM control as the primary means of actuation, but limited agility was the most that could be achieved when the maximum torque was limited to twice the rated continuous torque of the Hexacopter and Lift+Cruise configurations tested.

3. Transient torque requests to the motor controller from the flight control system during maneuvering flight were of an impulsive nature, with pulse durations less than 3 s. The predefined maximum torque limit was reached 3.9% of the flight time during the Lateral Reposition maneuvers.

4. Activation of electric powertrain saturation or rate limits in RPM-controlled eVTOL aircraft can lead to a sudden and severe (potentially catastrophic) deterioration of the handling qualities during aggressive maneuvering. The OLOP criterion, when determined from the broken loop responses at the motor torque commands, successfully predicted the possibility of torque saturation occurring.

5. Lower aggressiveness required by the Precision Hover HQTE generally, but not universally, resulted in lower (better) HQR values for the aircraft and control laws that were tested. Abruptness of the response and tendencies to over control that may have been caused by a heightened controller response sensitivity were more readily detected in the Hover MTE.

6. The trade-off in agility and precision required by the two Lateral Reposition tasks resulted in similar HQR for ACAH configurations, but the Lateral Precision and Hover HQTE allowed evaluation of TRC and the identification of potential HQ cliffs without loss of control departures.

Author contact: Carlos Malpica, carlos.a.malpica@nasa.gov

REFERENCES

1. Johnson, W., Silva, C., and Solis, E., "Concept Vehicles for VTOL Air Taxi Operations," Presented at the AHS Technical Conference on Aeromechanics Design for Transformative Vertical Flight, San Francisco, CA, January 16–19, 2018.

2. Silva, C., Johnson, W., Antcliff, K. R., and Patterson, M. D., "VTOL Urban Air Mobility Concept Vehicles for Technology Development," Paper AIAA 2018-3847, 2018 Aviation Technology, Integration, and Operations Conference, AIAA AVIATION Forum, Atlanta, GA, June 25–29, 2018.

3. Anonymous, "eVTOL Aircraft Directory," https://evtol.news/aircraft/, Accessed February 11, 2020.

4. National Academies of Sciences, Engineering, and Medicine, *Advancing Aerial Mobility: A National Blueprint*, The National Academies Press, Washington, DC, 2020. DOI: https://doi.org/10.17226/25646.

5. "Urban Air Mobility and Advanced Air Mobility," https://www.faa.gov/uas/advanced_operations/urban_air_mobility, Accessed January 25, 2023.

6. Walter, A., McKay, M., Niemiec, R., Gandhi, F., and Ivler, C., "Handling Qualities Based Assessment of Scalability for Variable-RPM Electric Multi-Rotor Aircraft," Proceedings of the 75th Annual Forum, Philadelphia, PA, May 13–16, 2019.

7. Welsch, M., and Fichter, W., "Control of Large Multicopters with Rate-Limited Electric Motors," AIAA SciTech Forum, Orlando, FL, January 6–10, 2020.

8. Malpica, C., and Withrow-Maser, S., "Handling Qualities Investigation of Variable Blade Pitch and Variable Rotor Speed Controlled eVTOL Quadrotor Concepts for Urban Air Mobility," Proceedings of the VFS International Powered Lift Conference 2020, San Jose, CA, January 21–23, 2020.

9. Walter, A., McKay, M., Niemiec, R., Gandhi, F., and Ivler, C., "Hover Handling Qualities of Fixed-Pitch,

Variable-RPM Quadcopters with Increasing Rotor Diameter," Proceedings of the 76th Annual Forum, Virtual, October 6–8, 2020.

10. Ivler, C. M., Hunter, W., Vo, E., Russell, K., Malpica, C., and Withrow-Maser, S., "Handling Qualities Considerations in Control Allocation for Multicopters," Proceedings of the 77th Annual Forum, Fort Worth, TX, May 10–12, 2022.

11. Anon., "Handling Qualities Requirements for Military Rotorcraft," Aeronautical Design Standard-33 (ADS-33E-PRF), US Army Aviation and Missile Command, March 2000.

12. Blanken, C. L., Tischler, M. B., Lusardi, J. A., Berger, T., Ivler, C. M., and Lehmann, R., "Proposed Revisions to Aeronautical Design Standard – 33E (ADS-33E-PRF) Toward ADS-33F-PRF," Special Report SR-FCDD-AMV-19-01, U.S. Army Combat Capabilities Development Command, September 2019.

13. Withrow-Maser, S., Aires, J., Ruan, A., Malpica, C., and Schuet, S., "Evaluation of Heave Disturbance Rejection and Control Response Criteria on the Handling Qualities of Urban Air Mobility (UAM) eVTOL Quadrotors Using the Vertical Motion Simulator," Proceedings of the Vertical Flight Society's Aeromechanics for Advanced Vertical Flight Technical Meeting, San Jose, CA, January 25–27, 2022.

14. Klyde, D. H., Schulze, P. C., Mitchell, D. G., Sizoo, D., Schaller, R., and McGuire, R., "Mission Task Element Development Process: An Approach to FAA Handling Qualities Certification," Paper AIAA 2020-3285, AIAA AVIATION 2020 FORUM, Virtual, June 15–19, 2020.

15. Klyde, D., Jones, M., Shubert, M., Mitchell, D., Schaller, R., Sizoo, D., Webber, D., van Houdt, J., Feary, M., and Simmons, R., "Towards Handling Qualities and Automation Assessment for Certification of eVTOL Aircraft," Vertical Flight Society's 78th Annual Forum Proceedings, Fort Worth, TX, May 10–12, 2022.

16. Aires, J., Withrow-Maser, S., Ruan, A., Malpica, C., and Schuet, S., "Analysis of Handling Qualities and Power Consumption for Urban Air Mobility (UAM) eVTOL Quadrotors with Degraded Heave Disturbance Rejection and Control Response," Proceedings of the Vertical Flight Society's 78th Annual Forum, Fort Worth, TX, May 10–12, 2022.

17. Brenner, F., O'Heron, P., Gomez, L. F., Goericke, J., and Hasbun, M., "Comprehensive Simulation for eVTOL Aircraft-Diagnosing Coupled Airframe-Propulsion Dynamic Instabilities," Vertical Flight Society's 78th Annual Forum Proceedings, Fort Worth, TX, May 10–12, 2022.

18. McRuer, D. T., Droste, C. S., Hansman, R. J., Jr., Hess, R. A., LeMaster, D. P., Matthews, S., McDonnell, J. D., McWha, J., Melvin, W. W., and Pew, R. W., "Aviation Safety and Pilot Control: Understanding and Preventing Unfavorable Pilot-Vehicle Interactions," Technical report, National Research Council, 1997.

19. Carpenter, P. J., and Friedovitch, B., "The Effect of a Rapid Blade Pitch Increase on the Thrust and Induced Velocity of a Full-Scale Helicopter Rotor," TN 3044, NACA, 1953.

20. Duda, H., "Prediction of Pilot-in-the-Loop Oscillations Due to Rate Saturation," *Journal of Guidance, Control, and Dynamics*, Vol. 20, (3), May–June 1997, pp. 581–587.

21. Jones, M., "The Use of the Open-Loop Onset Point (OLOP) to Predict Rotorcraft Pilot-Induced Oscillations," Proceedings of the 75th Annual Forum, Philadelphia, PA, May 13–16, 2019.

22. Johnson, W., "NDARC–NASA Design and Analysis of Rotorcraft," NASA/TP 2015-218751, National Aeronautics and Space Administration, April 2015.

23. Tischler, M. B., Colbourne, J. D., Morel, M. R., Biezad, D. J., Cheung, K. K., Levine, W. S., and Moldoveanu, V., "A Multidisciplinary Flight Control Development Environment and Its Application to a Helicopter," *IEEE Control Systems Magazine*, Vol. 19, (4), August 1999, pp. 22–33.

24. Hanson, C., Suh, P., Barnes, K., Malpica, C., Withrow-Maser, S., Aires, J., Schuet, S., Ruan, A., Altamirano, G., Foster, J., and Matt, J., "Test Report on the Pilot Handling Qualities Evaluation of Urban Air Mobility (UAM) Aircraft with High Augmentation Modes and Failures," NASA/TM 20230003386, NASA, to be published October 2023.

25. Aponso, B. L., Tran, D. T., Schroeder, J. A., and Beard, S. D., "Rotorcraft Research at the NASA Vertical Motion Simulator," Paper AIAA 2009-6056, AIAA Atmospheric Flight Mechanics Conference, Chicago, IL, August 10–13, 2009.

26. Hess, R., "Rotorcraft handling qualities in turbulence," *Journal of Guidance, Control, and Dynamics*, Vol. 18, (1,), 1995, pp. 39–45.

27. Anon., "Flying Qualities of Piloted Aircraft," Technical Report MIL-STD-1797A, U.S. Department of Defense, 1995.

28. Franklin, J. A., and Stortz, M. W., "Moving Base Simulation Evaluation of Translational Rate Command Systems for STOVL Aircrafst in Hover," Technical Memorandum 110399, NASA, June 1996.

29. Malpica, C. A., Theodore, C. R., Lawrence, B., and Blanken, C. L., "Handling Qualities of Large Rotorcraft in Hover and Low Speed," TP 2015–216656, NASA, March 2015.

30. Altamirano, G., Matt, J., Foster, J., Suh, P., Hanson, C., Malpica, C., and Schuet, S., "Flying Qualities Analysis and Piloted Simulation Testing of a Lift+Cruise Vehicle with Propulsion Failures in Hover and Low-Speed Conditions," Proceedings of the 79th Annual Forum, West Palm Beach, FL, May 16–18, 2023.

31. Krishnan, R., *Electric Motor Drives Modeling, Analysis, and Control*, Prentice Hall, Hoboken, New Jersey, 2001.

32. Wai, J., and Jahns, T. M., "A New Control Technique for Achieving Wide Constant Power Speed Operation with an Interior PM Alternator Machine," In IEEE Industry Applications Conference, Vol. 2, Chicago, IL, September 30–October 4, 2001.

33. Han, W., *Simulation Model Development of Electric Motor and Controller*, Master's thesis, Chalmers University of Technology, Gothenburg, Sweden, 2017.

34. Salyer, Z., *Thermal Models of Electric Powertrain Components for Cooling System Simulation and Design Requirements*, Undergraduate honors thesis, The Ohio State University, Columbus, Ohio, 2019.

35. Erdinc, O., Vural, B., and Uzunoglu, M., "A dynamic lithium-ion battery model considering the effects of temperature and capacity fading," IEEE 2009 International Conference on Clean Electrical Power, Capri, Italy, June 9–11, 2009.

36. Shabani, B., and Biju, M., "Theoretical Modelling Methods for Thermal Management of Batteries," *Energies*, Vol. 8, (9), 2015, pp. 10153–10177.

37. Cooper, G. E., and Harper, R. P., Jr., "The Use of Pilot Rating in the Evaluation of Aircraft Handling Qualities," Technical Note NASA TN D-5153, NASA, April 1969.